6. Kirino Y, Yasukawa T, Ohta S, Akira S, Ishihara K, Watanabe K (2004) Codon-specific translational defect caused by a wobble modification deficiency in mutant tRNA from a human mitochondrial disease. Proc Natl Acad Sci U S A 101:15070–15075
7. Kirino Y, Goto Y, Campos Y, Arenas J, Suzuki T (2005) Specific correlation between the wobble modification deficiency in mutant tRNAs and the clinical features of a human mitochondrial disease. Proc Natl Acad Sci U S A 102:7127–7132
8. Nelson I, Hanna MG, Alsanjari N, Scaravilli F, Morgan-Hughes JA, Harding AE (1995) A new mitochondrial DNA mutation associated with progressive dementia and chorea: a clinical, pathological, and molecular genetic study. Ann Neurol 37:400–403
9. Santorelli FM, Tanji K, Sano M, Shanske S, El-Shahawi M, Kranz-Eble P (1997) Maternally inherited encephalopathy associated with a single-base insertion in the mitochondrial $tRNA^{Trp}$ gene. Ann Neurol 42:256–260
10. Silvestri G, Rana M, DiMuzio A, Uncini A, Tonali P, Servidei S (1998) A late-onset mitochondrial myopathy is associated with a novel mitochondrial DNA (mtDNA) point mutation in the $tRNA^{Trp}$ gene. Neuromuscul Disord 8:291–295
11. Maniura-Weber K, Taylor RW, Johnson MA, Chrzanowska-Lightowlers Z, Morris AA, Charlton CP (2004) A novel point mutation in the mitochondrial $tRNA^{Trp}$ gene produces a neurogastrointestinal syndrome. Eur J Hum Genet 12:509–512
12. Sacconi S, Salviati L, Nishigaki Y, Walker WF, Hernandez-Rosa E, Trevisson E (2008) A functionally dominant mitochondrial DNA mutation. Hum Mol Genet 17:1814–1820
13. Mkaouar-Rebai E, Chamkha I, Kammoun F, Kammoun T, Aloulou H, Hachicha M (2009) Two new mutations in the MT-TW gene leading to the disruption of the secondary structure of the $tRNA^{Trp}$ in patients with Leigh syndrome. Mol Genet Metab 97:179–184
14. Sproule DM, Kaufmann P (2008) Mitochondrial encephalopathy, lactic acidosis, and strokelike episodes: basic concepts, clinical phenotype, and therapeutic management of MELAS syndrome. Ann NY Acad Sci 1142:133–158
15. Takahashi K, Tanabe K, Ohnuki M, Narita M, Ichisaka T, Tomoda K (2007) Induction of pluripotent stem cells from adult human fibroblasts by defined factors. Cell 131:861–872
16. Yu J, Vodyanik MA, Smuga-Otto K, Antosiewicz-Bourget J, Frane JL, Tian S (2007) Induced pluripotent stem cell lines derived from human somatic cells. Science 318:1917–1920
17. Akanuma J, Muraki K, Komaki H et al (2000) Two pathogenic point mutations exist in the authentic mitochondrial genome, not in the nuclear pseudogene. J Hum Genet 45:337–341
18. Tanaka M, Takeyasu T, Fuku N, Li-Jun G, Kurata M (2004) Mitochondrial genome single nucleotide polymorphisms and their phenotypes in the Japanese. Ann NY Acad Sci 1011:7–20
19. Tsukihara T, Aoyama H, Yamashita E, Tomizaki T, Yamaguchi H, Shinzawa-Itoh K (1996) The whole structure of the 13-subinit oxidized cytochrome *c* oxidase at 2.8 A. Science 272:1136–1144
20. Trounce IA, Kim YL, Jun AS, Wallace DC (1996) Assessment of mitochondrial oxidative phosphorylation in patient muscle biopsies, lymphoblasts, and transmitochondrial cell lines. Methods Enzymol 264:484–509
21. Schägger H (2006) Tricine-SDS-PAGE. Nat Protocol 1:16–22
22. Wittig I, Braun HP, Schägger H (2006) Blue native PAGE. Nat Protocol 1:418–428
23. Okita K, Matsumura Y, Sato Y, Okada A, Morizane A, Okamoto S (2011) A more efficient method to generate integration-free human iPS cells. Nat Methods 8:409–412
24. Chambers SM, Fasano CA, Papapetrou EP, Tomishima M, Sadelain M, Studer L (2009) Highly efficient neural conversion of human ES and iPS cells by dual inhibition of SMAD signaling. Nat Biotechnol 27:275–280
25. Menendez L, Yatskievych TA, Antin PB, Dalton S (2011) Wnt signaling and a Smad pathway blockade direct the differentiation of human pluripotent stem cells to multipotent neural crest cells. Proc Natl Acad Sci U S A 108:19240–19245
26. Blakely EL, Yarham JW, Alston CL, Craig K, Poulton J, Brierley C (2013) Pathogenic mitochondrial tRNA point mutations: nine novel mutations affirm their importance as a cause of mitochondrial disease. Hum Mutat 34:1260–1268
27. Armstrong L, Tilgner K, Saretzki G et al (2010) Human induced pluripotent stem cell lines show stress defense mechanisms and mitochondrial regulation similar to those of human embryonic stem cells. Stem Cells 28:661–673
28. Prigione A, Fauler B, Lurz R, Lehrach H, Adjaye J (2010) The senescence-related mitochondrial/oxidative stress pathway is repressed in human induced pluripotent stem cells. Stem Cells 28:721–733
29. Folmes CD, Nelson TJ, Martinez-Fernandez A, Arrell DK, Lindor JZ, Dzeja PP (2011) Somatic oxidative bioenergetics transitions into pluripotency-dependent glycolysis to facilitate nuclear reprogramming. Cell Metab 14:264–271
30. Folmes CD, Dzeja PP, Nelson TJ, Terzic A (2012) Metabolic plasticity in stem cell homeostasis and differentiation. Cell Stem Cell 11:596–606
31. Shoubridge EA (2001) Cytochrome *c* oxidase deficiency. Am J Med Genet 106:46–52
32. Silvestri G, Mongini T, Odoardi F, Modoni A, De Rosa G, Doriguzzi C (2000) A new mtDNA mutation associated with a progressive encephalopathy and cytochrome *c* oxidase deficiency. Neurology 54:1693–1696
33. Fujikura J, Nakao K, Sone M, Noguchi M, Mori E, Naito M (2012) Induced pluripotent stem cells generated from diabetic patients with mitochondrial DNA A3243G mutation. Diabetologia 55:1689–1698
34. Cherry AB, Gagne KE, McLoughlin EM, Baccei A, Gorman B, Hartung O (2013) Induced pluripotent stem cells with a mitochondrial DNA deletion. Stem Cells 31:1287–1297
35. Folmes CD, Martinez-Fernandez A, Perales-Clemente E, Li X, McDonald A, Oglesbee D (2013) Disease-causing mitochondrial heteroplasmy segregated within induced pluripotent stem cell clones derived from a patient with MELAS. Stem Cells 31:1298–1308
36. Hämäläinen RH, Manninen T, Koivumäki H, Kislin M, Otonkoski T, Suomalainen A (2013) Tissue- and cell-type-specific manifestations of heteroplasmic mtDNA 3243A > G mutation in human induced pluripotent stem cell-derived disease model. Proc Natl Acad Sci U S A 110:E3622–E3630
37. Kodaira M, Hatakeyama H, Yuasa S, Seki T, Egashira T, Tohyama S (2015) Impaired respiratory function in MELAS-induced pluripotent stem cells with high heteroplasmy levels. FEBS Open Bio 5:219–225

ELSEVIER

Brain & Development 37 (2015) 719–724

BRAIN & DEVELOPMENT
Official Journal of the Japanese Society of Child Neurology

www.elsevier.com/locate/braindev

Case Report

Myocerebrohepatopathy spectrum disorder due to *POLG* mutations: A clinicopathological report

Hesham Montassir [a,b], Yoshihiro Maegaki [a,*], Kei Murayama [c], Taro Yamazaki [d], Masakazu Kohda [e], Akira Ohtake [d], Hiroyasu Iwasa [e], Yukiko Yatsuka [f], Yasushi Okazaki [e,f], Chitose Sugiura [a], Ikuo Nagata [g], Mitsuo Toyoshima [h], Yoshiaki Saito [a], Masayuki Itoh [i], Ichizo Nishino [j], Kousaku Ohno [a]

[a] *Division of Child Neurology, Faculty of Medicine, Tottori University, Yonago, Japan*
[b] *Department of Family Medicine, Faculty of Medicine, Cairo University, Cairo, Egypt*
[c] *Department of Metabolism, Chiba Children's Hospital, Chiba, Japan*
[d] *Department of Pediatrics, School of Medicine, Saitama Medical University, Saitama, Japan*
[e] *Division of Translational Research, Research Center for Genomic Medicine, Saitama Medical University, Hidaka, Japan*
[f] *Division of Functional Genomics & Systems Medicine, Research Center for Genomic Medicine, Saitama Medical University, Hidaka, Japan*
[g] *Division of Pediatrics and Perinatology, Faculty of Medicine, Tottori University, Yonago, Japan*
[h] *Department of Pediatrics, Graduate School of Medical and Dental Sciences, Kagoshima University, Kagoshima, Japan*
[i] *Department of Mental Retardation and Birth Defect Research, National Center of Neurology and Psychiatry, Tokyo, Japan*
[j] *Department of Neuromuscular Research, National Institute of Neuroscience, National Center of Neurology and Psychiatry, Tokyo, Japan*

Received 8 August 2014; received in revised form 6 October 2014; accepted 26 October 2014

Abstract

We report on the clinical, neuropathological, and genetic findings of a Japanese case with myocerebrohepatopathy spectrum (MCHS) disorder due to polymerase gamma (*POLG*) mutations. A girl manifested poor sucking and failure to thrive since 4 months of age and had frequent vomiting and developmental regression at 5 months of age. She showed significant hypotonia and hepatomegaly. Laboratory tests showed hepatocellular dysfunction and elevated protein and lactate levels in the cerebrospinal fluid. Her liver function and neurologic condition exacerbated, and she died at 8 months of age. At autopsy, fatty degeneration and fibrosis were observed in the liver. Neuropathological examination revealed white matter-predominant spongy changes with Alzheimer type II glia and loss of myelin. Enzyme activities of the respiratory chain complex I, III, and IV relative to citrate synthase in the muscle were normal in the biopsied muscle tissue, but they were reduced in the liver to 0%, 10%, and 14% of normal values, respectively. In the liver, the copy number of mitochondrial DNA compared to nuclear DNA was reduced to 3.3% of normal values as evaluated by quantitative polymerase chain reaction. Genetic analysis revealed compound heterozygous mutations for *POLG* (I1185T/A957V). This case represents the differential involvement of multiple organs and phenotype-specific distribution of brain lesions in mitochondrial DNA depletion disorders.

Keywords: Alpers syndrome; Mitochondrial DNA depletion; Myocerebrohepatopathy spectrum disorder; *POLG*

* Corresponding author at: Division of Child Neurology, Faculty of Medicine, Tottori University, 36-1 Nishi-Cho, Yonago 683-8504, Japan. Tel.: +81 859 38 6777; fax: +81 859 38 6779.
E-mail address: maegaki@med.tottori-u.ac.jp (Y. Maegaki).

http://dx.doi.org/10.1016/j.braindev.2014.10.013
0387-7604/

1. Introduction

Mitochondrial DNA (mtDNA) depletion syndrome (MDDS), first described in 1991, is defined as a reduction in the mtDNA copy number in different tissues, leading to insufficient synthesis of respiratory chain complexes (RCC) [1]. Clinical manifestations of MDDS involve many organ systems including the central and peripheral nervous system, liver, muscle, and gastrointestinal tract [2]. Human polymerase gamma (*POLG*) is the common causative gene involved in MDDS, whose mutations result in a diverse group of phenotypes, such as Alpers syndrome and myocerebrohepatopathy spectrum (MCHS) disorders, which typically show disease onset during early childhood. Further, several *POLG*-related phenotypes manifesting during adolescence and adulthood are recognized, including progressive external ophthalmoplegia, ataxia-neuropathy spectrum disorders, myoclonus epilepsy myopathy sensory ataxia, and sensory ataxic neuropathy with dysarthria/dysphagia and ophthalmoplegia. Some overlaps in the symptoms between these adult phenotypes exist, and can be additionally accompanied by tremor, parkinsonism, hearing loss, stroke-like episodes, and gastrointestinal symptoms, which are reminiscent of symptoms of mitochondrial diseases with pathomechanisms other than MDDS [3,4].

MCHS, the most severe phenotype of POLG disorders, was recently identified and is defined by the clinical triad of (1) myopathy or hypotonia, (2) developmental delay or dementia, and (3) liver dysfunction [3,5]. Severe, intractable epilepsy is included in the diagnostic hallmarks of Alpers syndrome, but is not characteristic of MCHS. As the number of patients with MCHS disorders is small and detailed clinicopathological findings are unavailable, we herein report the case of a girl with MCHS disorders due to *POLG* mutations. As far as we know, this is the first Japanese case of MCHS disorders with *POLG* mutation.

2. Case report

A girl was born at 40 weeks of gestation to healthy non-consanguineous parents without any abnormalities. The birth weight, height, and head circumference were normative. Early development and growth were unremarkable. At 4 months of age, she developed poor weight gain, emesis, hypotonia, developmental delay, and lethargy. She was admitted to our hospital because of recurrent vomiting at 6 months of age.

On admission, body length was 60.9 cm [−2.2 standard deviation (SD)], body weight was 5600 g (−2.3 SD), and head circumference was 42 cm (+0.2 SD). Hepatomegaly of a hard consistency was observed approximately 3 cm under the costal margin with no associated splenomegaly. She was alert and could establish good eye contact and smile. She showed severe hypotonia and proximal dominant muscular weakness. She could hold neither her head nor limbs up. All deep tendon reflexes were weak.

Although complete blood count and urinalysis were unremarkable, hepatocellular dysfunction was obvious at the time of hospitalization, with the following laboratory test values: aspartate aminotransferase, 390 U/L; alanine aminotransferase, 218 U/L; total bilirubin, 1.6 mg/dL; total bile acids, 172 μmol/L; γ-glutamyl transpeptidase, 179 IU/L; leucine aminopeptidase, 268 IU/L; and cholinesterase, 73 IU/L. Levels of serum creatine kinase and blood glucose were normal. Cerebrospinal fluid (CSF) examination showed elevated protein levels of 304 mg/dL and normal cell count and glucose levels. Lactic acid was elevated in both plasma and CSF, at 15.9 mg/dL and 30.3 mg/dL, respectively. Pyruvic acid was normal in both plasma and CSF. Metabolic screening tests, including urine organic acids, plasma, and urine amino acids, were unremarkable. Initial brain computed tomography (CT) and magnetic resonance imaging performed at 6 months of age were unremarkable. The electroencephalogram showed generalized slow wave activity. Only wave I was identifiable on auditory evoked potentials. Motor nerve and sensory conduction were mildly delayed.

Muscle biopsy findings at 6 months of age showed a variation in fiber type; ragged-red fiber was not observed. Lipid and glycogen storage were not observed. Cytochrome c oxidase staining showed normal findings. Analysis of the RCC enzyme activity revealed no abnormality. No mtDNA mutations were identified.

Soon after admission, difficulty in feeding and vomiting aggravated, and tube feeding along with parenteral nutrition was required. She experienced bouts of diarrhea. Consciousness level decreased progressively, and myoclonic jerks of the right and left arms were infrequently observed. Follow-up CT revealed mild cerebral atrophy at 7 months of age. Hepatocellular dysfunction exacerbated progressively, and she died of multiple organ failure caused by hepatic failure at 8 months of age, despite supplementation of multiple vitamins and coenzyme Q 10, and was autopsied. Two years later, another girl was born to the parents. She had the same clinical course and laboratory findings observed in the present patient and died at 7 months of age. Valproic acid was not used in either patient.

2.1. Postmortem examinations

Body weight was 6.0 kg (mean ± SD, 8.0 ± 0.88 kg). The weight of the atrophic liver was 200 g, and the surface was yellowish, irregular, and hard. The lungs were congested and adrenal glands were atrophic. The other visceral organs were unremarkable on macroscopic

examination. The brain weighed 760 g and showed massive edema and caudal necrosis. Microscopically, hepatocytes and adrenal cortical cells were swollen, and renal tubular cells contained phospholipids and diffuse foam cells. Similar foam cells were also seen in the lungs and cardiac muscle fibers. In the liver, hepatic fibrosis, microvesicular steatosis, and fatty degeneration were observed (Fig. 1). In the central nervous system, a spongy change was noted predominantly in the cerebral white matter, and neuronal loss in the cerebral and cerebellar cortex was mild. Alzheimer type II glia was observed in massive numbers in the cerebral and cerebellar white matter, with a smaller amount in the cerebral cortex and deep gray matter. Neuronal loss, capillary proliferation, and sponginess were prominent in the substantia nigra (Fig. 2). Recent linear necrosis was present in the bilateral caudate nucleus.

2.2. Assay of respiratory chain complex enzyme activity in the liver

The liver samples were immediately frozen at autopsy and stored at −70 °C. Activities of RCC I, II, III and IV were assayed as described previously [6,7]. The percentages of RCC I, II, III and IV activities relative to that of citrate synthase (CS) as a mitochondrial enzyme marker were calculated. Relative enzyme activities of RCC I, III, and IV to CS in the liver were reduced to 0%, 10%, and 14% of normal values, respectively, while that of RCC II was reduced to 29%.

2.3. Analysis of quantitative polymerase chain reaction of mtDNA and DNA sequence of POLG gene

Written informed consent was obtained from the patient's parents in order to perform gene analysis. The quantitative estimation of mtDNA was performed by real-time amplification of fragments of *ND1* in the mtDNA genome, as previously described [7,8]. To determine the overall abundance of mtDNA, we compared the real-time amplification of *ND1* with a single-copy nuclear reference gene (exon 24 of the *CFTR* gene) [7,9]. The ratio of *ND1* to *CFTR* in the liver was reduced to 3.3% (SD, 1.2%) as compared to the control.

Mutation analysis was performed on the genomic DNA using primers designed to amplify the coding exons and the exon-intron boundaries of *POLG* (NM_002693.2). Fragments were analyzed by direct sequencing using ABI 3130XL (Applied Biosystems, Tokyo, Japan). The genetic analysis revealed compound heterozygous mutations in *POLG* (c.2870C>T, p.A957V and c.3554T>C, p.I1185T). The two DNA mutations

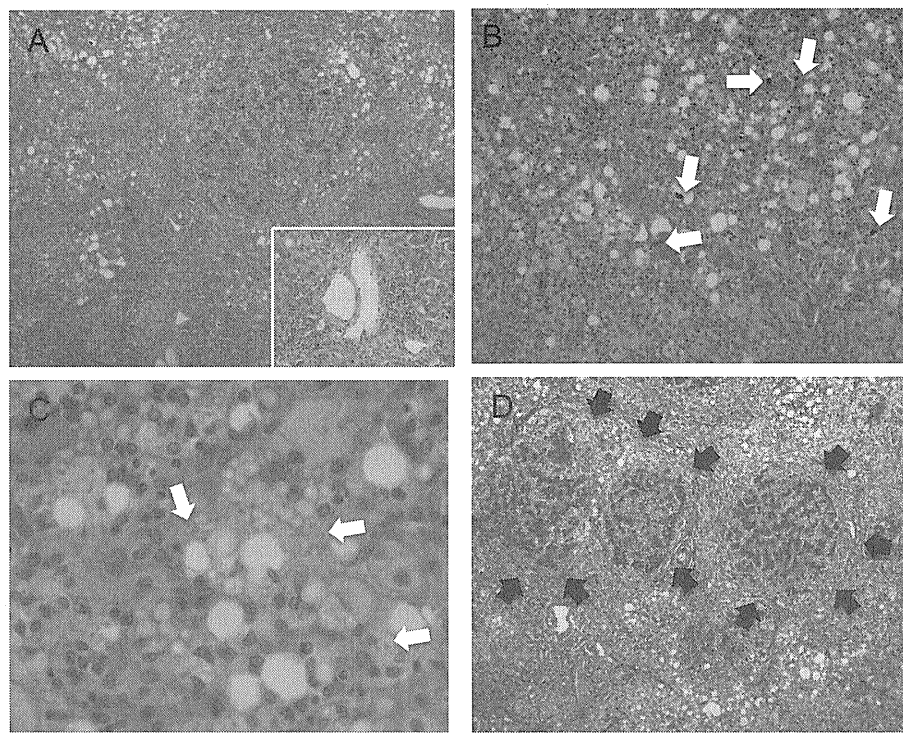

Fig. 1. Pathological findings of the postmortem liver (A–C: hematoxylin & eosin staining, D: Masson trichrome staining). (A) Moderate inflammatory cell infiltration (inset) with destroyed limiting plates and a rather progressive fibrosis with bridging formation in the portal tracts were observed (original magnification, ×40). (B) Swollen hepatocytes containing lipid droplets of various sizes were found. Bile plugs (white arrows in B and C) were noted in the cytoplasm of hepatocytes and dilated canaliculi (×100). (C) Swollen hepatocytes containing lipid droplets of various sizes were found. Bile plugs were noted in the cytoplasm of hepatocytes (×400). (D) A rather progressive fibrosis with bridging formation (arrows) in the portal tracts was found (×40).

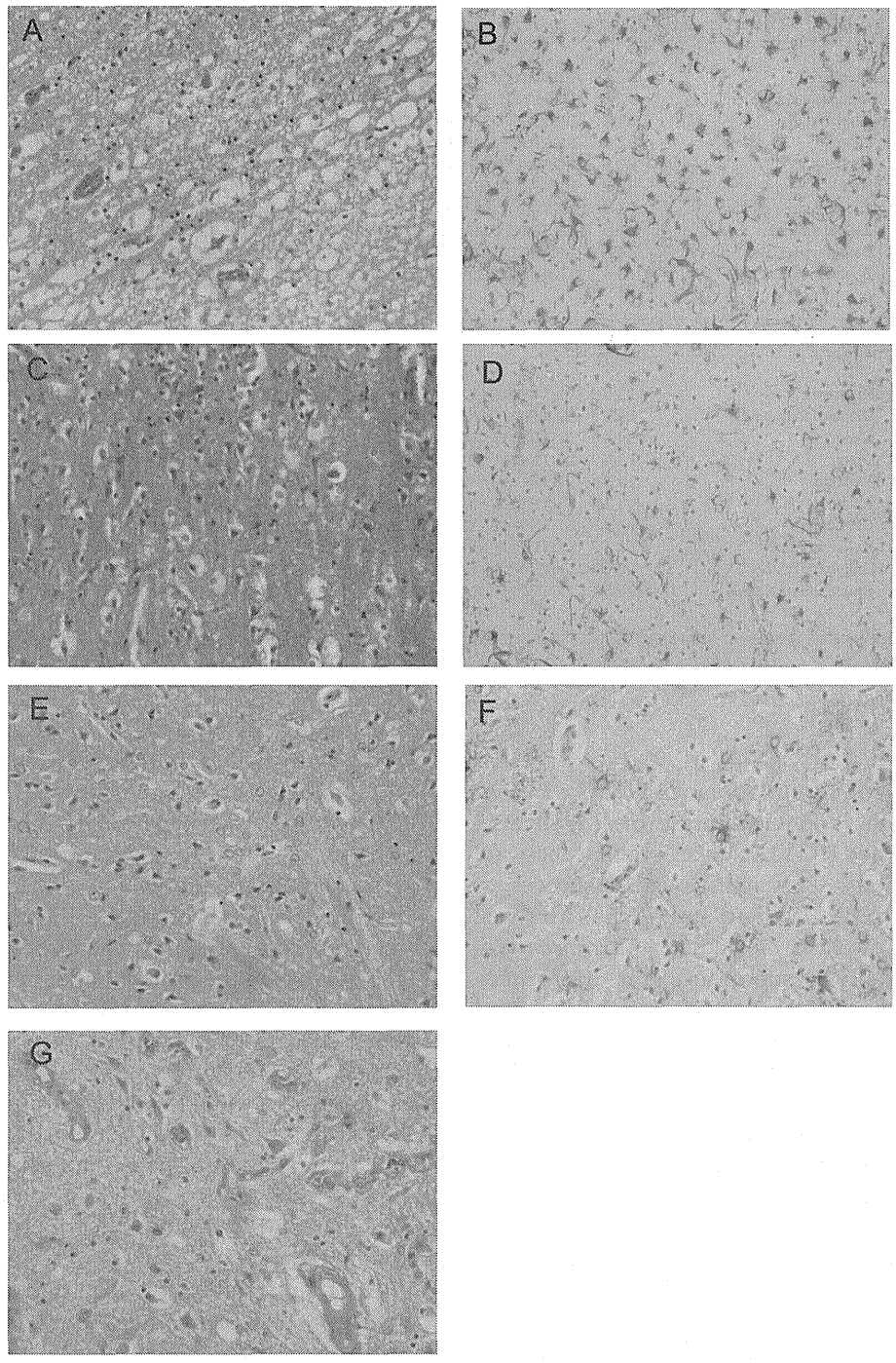

Fig. 2. Pathological findings of the postmortem brain (A, C, E, and G: hematoxylin & eosin staining; B, D, and F: immunohistochemical staining against glial fibrillary acidic protein; original magnification, ×400). Marked spongy changes (A) with Alzheimer type II astrocytosis (B) was observed in the cerebral white matter, and less prominently in the cerebral cortex (C and D) and striatum (E and F). Neuronal loss, sponginess, and capillary proliferation, which were reminiscent of the findings of Leigh syndrome, were noted in the substantia nigra (G).

were not registered in neither of the 1000 Genomes Project Database (http://www.1000genomes.org/), ESP6500 database (http://evs.gs.washington.edu/EVS/) or HGVD (http://www.genome.med.kyoto-u.ac.jp/SnpDB/index.html). The amino acid sequences of these two sites (p.A957V and p.I1185T) are well conserved across species, suggesting their importance (Fig. 3). *In silico* analyses were performed using the prediction algorithms SIFT (http://sift.jcvi.org) and PolyPhen2 (http://genetics.bwh.harvard.edu/pph2/). These mutations are predicted to be deleterious by SIFT (0 and 0, respectively) and PolyPhen2 (0.985 and 0.991, respectively) programs. The results of mutation analysis have been reported previously (patient 6 in Ref. [9]).

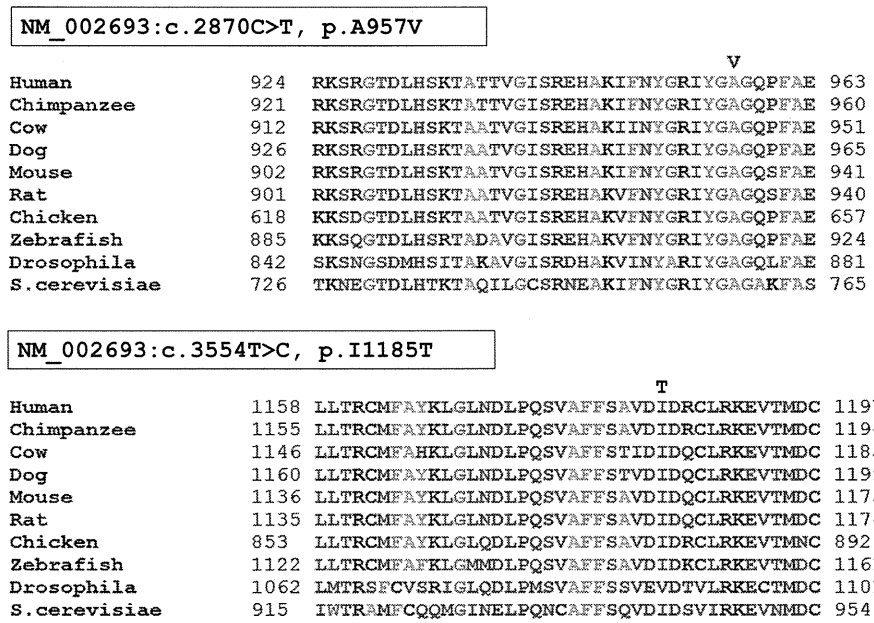

Fig. 3. Conservation analysis of mutation sites in *POLG*. The sites of compound heterozygous amino acid mutations (p.957A and p.1185I) are well conserved across species.

3. Discussion

The hetero compound mutations in *POLG* were not found in either of the 1000 Genomes Project Database, ESP6500 database nor HGVD, suggesting that these are pathogenic mutations. The amino acid sequences of these two sites (p.A957V and p.I1185T) are well conserved across species including *Saccharomyces cerevisiae*, indicating their importance (Fig. 3). *In silico* analyses also predicted that these two amino acid mutations are deleterious. Furthermore A957V has been reported by Tang et al. [10]. They reported A957V allele was shared in three unrelated patients and concluded this mutation is pathogenic. The pathogenic mutations in the flanking region of p.1185I; p.1184D [11,12] and p.1186D [13] have been reported, suggesting this region is also important. Thus, we conclude the compound heterozygous mutations of this patient cause the disease.

Alpers syndrome is defined as the clinical triad of (1) refractory, mixed-type seizures that often include a focal component, (2) psychomotor regression, often triggered by intercurrent infection, and (3) hepatopathy with or without acute liver failure. There is an overlap between the phenotypes of MCHS and Alpers syndrome; however, the former usually shows an earlier onset age and more rapid disease progression, while the latter is characterized by intractable epilepsy. Using the "myo-" prefix in MCHS may be confusing since the pathological findings of muscles in this disorder often shows no evidence of mitochondrial myopathy; instead, the hypotonia observed in the triad can be regarded as a symptom of brain dysfunction. Thus, the clinical features of the patient discussed herein were typical of MCHS.

Although Wong et al. [3] "*...excluded classical Alpers hepatopathy by liver biopsy*" in MHCS, exact pathological findings were not provided by the authors. Differences in the hepatopathy observed in these two phenotypes have not been established; pathological characteristics of the liver in Alpers syndrome include fibrosis, regenerative nodules, hepatocyte dropout, bile duct proliferation, fatty changes, and bile stasis [14]. The findings of the present patient were compatible with those of Alpers syndrome, similar to the case of POLG-related MDDS previously observed [15]. As for the neuropathological findings, Alpers syndrome usually shows a preferential involvement of gray matter, characterized by gliosis, nerve cell loss, spongy degeneration, and accumulation of neural lipids in the cerebral cortex [16]. Alzheimer type II glia, representing hepatic encephalopathy, was also distributed predominantly in the gray matter [17].

A patient exhibiting a clinical evolution from MCHS to Alpers phenotype showed gray matter involvement and microscopic findings similar to those in Leigh syndrome [5], and brain biopsy in another Alpers patient with prominent white matter signal change revealed pathological characteristics typical of Alpers disease with intractable seizures [18]. On the other hand, marked gliosis and sponginess of the white matter without pathological changes in the cerebral cortex was observed in a patient with probable MCHS [17]. Apart from these, we could not find any MCHS cases with a neuropathological description in the literature. The white matter-predominant spongy degeneration with Alzheimer type II astrocytosis in the present patient may therefore be characteristic of MCHS.

POLG disorders often show elevated levels of lactate both in the serum and CSF as well as elevated levels of hepatic enzymes. However, these findings are not specific for POLG disorders; rather, they are hallmarks of mitochondrial disorders. Analysis of the RCC enzyme activity is the most valuable test for diagnosis of MDDS. However, RCC enzyme activity varies among muscle, liver, kidney, and brain tissues in the same patient [1,19], presumably due to the differential degree of DNA depletion among individual organs. The constituents of complex II are coded by genes in the nuclear, not mitochondrial DNA. In the present patient, the decreased complex II enzyme activity in the biopsied liver may either result from augmented activity of control CS enzyme due to an increase of mitochondria in number, or may be secondary to the damage of hepatocytes with necrotic and fibrotic changes [19]. It is very important to keep in mind that morphological findings and RCC enzyme activities in the muscle are sometimes unremarkable in MCHS patients, even though they show hypotonia or muscular weakness, as in the present case [5,15,20]. Therefore, analysis of RCC enzyme activities in the liver should be considered when Alpers syndrome or MCHS disorders are suspected, even when the morphological findings of muscle or enzyme assay results are unremarkable.

Acknowledgements

This study was supported in part by a grant from the Research Program of Innovative Cell Biology by Innovative Technology (Cell Innovation), a Grant-in-Aid for the Development of New Technology from The Promotion and Mutual Aid Corporation for Private Schools of Japan from MEXT (to Y. Okazaki), Grants-in-Aid for the Research on Intractable Diseases (Mitochondrial Disease) from the Ministry of Health, Labour and Welfare of Japan to A. Ohtake. Dr Murayama was supported by the Kawano Masanori Memorial Public Interest Incorporated Foundation for Promotion of Pediatrics.

References

[1] Moraes C, Shanske S, Tritschler HJ, Aprille JR, Andreetta F, Bonilla E, et al. mtDNA depletion with variable tissue expression: a novel genetic abnormality in mitochondrial diseases. Am J Hum Genet 1991;48:492–501.

[2] Sarzi E, Bourdon A, Chrétien D, Zarhrate M, Corcos J, Slama A, et al. Mitochondrial DNA depletion is a prevalent cause of multiple respiratory chain deficiency in childhood. J Pediatr 2007;150(531–4):e6.

[3] Wong L-J, Naviaux RK, Brunetti-Pierri N, Zhang Q, Schmitt ES, Truong C, et al. Molecular and clinical genetics of mitochondrial diseases due to *POLG* mutations. Hum Mutat 2008;29:150–72.

[4] Cohen BH, Naviaux RK. The clinical diagnosis of POLG disease and other mitochondrial DNA depletion disorders. Methods 2010;51:364–73.

[5] Scalais E, Francois B, Schlesser P, Stevens R, Nuttin C, Martin J-J, et al. Polymerase gamma deficiency (POLG): clinical course in a child with a two stage evolution from infantile myocerebrohepatopathy spectrum to an Alpers syndrome and neuropathological findings of Leigh's encephalopathy. Eur J Paediatr Neurol 2012;16:542–8.

[6] Kirby DM, Crawford M, Cleary MA, Dahl HH, Dennett X, Tourburn DR. Respiratory chain complex I deficiency. An underdiagnosed energy generation disorder. Neurology 1999;52:1255–64.

[7] Kaji S, Murayama K, Nagata I, Nagasaka H, Takayanagi M, Ohtake A, et al. Fluctuating liver functions in siblings with MPV17 mutations and possible improvement associated with dietary and pharmaceutical treatments targeting respiratory chain complex II. Mol Genet Metab 2009;97:292–6.

[8] Pagnamenta AT, Taanman JW, Wilson CJ, Anderson NE, Marotta R, Duncan AJ, et al. Dominant inheritance of premature ovarian failure associated with mutant mitochondrial DNA polymerase gamma. Hum Reprod 2006;21:2467–73.

[9] Yamazaki T, Murayama K, Compton AG, Sugiana C, Harashima H, Amemiya S, et al. Molecular diagnosis of mitochondrial respiratory chain disorders in Japan: focusing on mitochondrial DNA depletion syndrome. Pediatr Int 2014;56:180–7.

[10] Tang S, Wang J, Lee NC, Milone M, Halberg MC, Schmitt ES, et al. Mitochondrial DNA polymerase gamma mutations: an ever expanding molecular and clinical spectrum. J Med Genet 2011;48:669–81.

[11] Martikainen MH, Hinttala R, Majamaa K. Novel POLG1 mutations in a patient with adult-onset progressive external ophthalmoplegia and encephalopathy. BMJ Case Reports 2010; doi:10.1336/bcr.01.2010.2604.

[12] González-Vioque E, Blázquez A, Fernández-Moreira D, Bornstein B, Bautista J, Arpa J, et al. Association of novel POLG mutations and multiple mitochondrial DNA deletions with variable clinical phenotypes in a Spanish population. Arch Neurol 2006;63:107–11.

[13] Cheldi A, Ronchi D, Bordoni A, Bordo B, Lanfranconi S, Bellotti MG, et al. *POLG1* mutations and stroke like episodes: a distinct clinical entity rather than an atypical MELAS syndrome. BMC Neurol 2013;13:8.

[14] Nguyen KV, Sharief FS, Chan SS, Copeland WC, Naviaux RK. Molecular diagnosis of Alpers syndrome. J Hepatol 2006;45:108–16.

[15] Kurt B, Jaeken J, Van Hove J, Lagae L, Löfgren A, Everman DB, et al. A novel POLG gene mutation in 4 children with Alpers-like hepatocerebral syndromes. Arch Neurol 2010;67:239–44.

[16] Boustany R, Zucker A. Degenerative disease primarily gray matter. In: Swaiman KF, Ashwal S, Ferriero D, editors. Pediatric neurology: principles & practice. Philadelphia: Mosby; 2006. p. 1326–8.

[17] Kollberg G, Moslemi AR, Darin N, Nennesmo I, Bjarnadottir I, Uvebrant P, et al. POLG1 mutations associated with progressive encephalopathy in childhood. J Neuropathol Exp Neurol 2006;65:758–68.

[18] Bao X, Wu Y, Wong LJ, Zhang Y, Xiong H, Chou PC, et al. Alpers syndrome with prominent white matter changes. Brain Dev 2008;30:295–300.

[19] de Vries M, Rodenburg RJ, Morava E, van Kaauwen E, ter Laak H, Mullaart R, et al. Multiple oxidative phosphorylation deficiencies in severe childhood multi-system disorders due to polymerase gamma (*POLG1*) mutations. Eur J Pediatr 2007;166:229–34.

[20] Ferrari G, Lamantea E, Donati A, Filosto M, Briem E, Carrara F, et al. Infantile hepatocerebral syndromes associated with mutations in the mitochondrial DNA polymerase-gamma A. Brain 2005;128:723–31.

The American Journal of Pathology, Vol. 185, No. 6, June 2015

ELSEVIER

The American Journal of
PATHOLOGY

ajp.amjpathol.org

NEUROBIOLOGY

Property of Lysosomal Storage Disease Associated with Midbrain Pathology in the Central Nervous System of *Lamp-2*—Deficient Mice

Akiko Furuta,* Hisae Kikuchi,† Hiromi Fujita,† Daisuke Yamada,† Yuuki Fujiwara,†‡ Tomohiro Kabuta,† Ichizo Nishino,§ Keiji Wada,† and Yasuo Uchiyama*

From the Department of Cellular and Molecular Neuropathology, Juntendo University Graduate School of Medicine, Tokyo; the Departments of Degenerative Neurological Diseases† and Neuromuscular Research,§ National Institute of Neuroscience, National Center of Neurology and Psychiatry, Kodaira, Tokyo; and the Department of Electrical Engineering and Bioscience,‡ Graduate School of Advanced Science and Engineering, Waseda University, Shinjuku, Tokyo, Japan*

Accepted for publication February 12, 2015.

Address correspondence to Akiko Furuta, M.D., Ph.D., Department of Cellular and Molecular Neuropathology, Juntendo University Graduate School of Medicine, Hongo 2-1-1, Bunkyo-ku, Tokyo 113-8421, Japan. E-mail: afuruta@juntendo.ac.jp.

Lysosome-associated membrane protein-2 (*LAMP-2*) is the gene responsible for Danon disease, which is characterized by cardiomyopathy, autophagic vacuolar myopathy, and variable mental retardation. To elucidate the function of LAMP-2 in the central nervous system, we investigated the neuropathological changes in *Lamp-2*—deficient mice. Immunohistochemical observations revealed that Lamp-1 and cathepsin D—positive lysosomal structures increased in the large neurons of the mouse brain. Ubiquitin-immunoreactive aggregates and concanavalin A—positive materials were detected in these neurons. By means of ultrastructural studies, we found various-shaped accumulations, including lipofuscin, glycolipid-like materials, and membranous structures, in the neurons and glial cells of *Lamp-2*—deficient brains. In deficient mice, glycogen granules accumulated in hepatocyte lysosomes but were not observed in neurons. These pathological features indicate lysosomal storage disease; however, the findings are unlikely a consequence of deficiency of a single lysosomal enzyme. Although previous study results have shown a large amount of autophagic vacuoles in parenchymal cells of the visceral organs, these findings were rarely detected in the brain tissue except for some axons in the substantia nigra, in which abundant activated microglial cells with increased lipid peroxidation were observed. Thus, LAMP-2 in the central nervous system has a possible role in the degradation of the various macromolecules in lysosomes and an additional function concerning protection from oxidative stress, especially in the substantia nigra. *(Am J Pathol 2015, 185: 1713—1723; http://dx.doi.org/10.1016/j.ajpath.2015.02.015)*

X-linked vacuolar cardiomyopathy and myopathy (Danon disease) are caused by the primary deficiency of lysosome-associated membrane protein-2 (LAMP-2).[1] Danon disease was first described as lysosomal glycogen storage disease with normal acid maltase because the cases closely resembled features of the infantile form of acid maltase deficiency (Pompe disease; glycogen storage disease type II), except that acid maltase activity was normal in the muscle.[2] The muscle malfunction of Danon disease has been well investigated with biopsied specimens characterized by autophagic vacuolar myopathy with sarcolemmal features.[3,4] Despite

Supported in part by Grant-in-Aid for Scientific Research (C) 23590244 from the Ministry of Education, Culture, Sports, Science and Technology (A.F.), Grant-in-Aid for Scientific Research 25290027 from the Japan Society for the Promotion of Science (K.W.), Grants-in-Aid for Scientific Research 05-32 from the Program for Promotion of Fundamental Studies in Health Sciences of the National Institute of Biomedical Innovation, Japan (K.W.), Grant-in-Aid for Creative Scientific Research 16GS0315 and Grants-in-Aid for Scientific Research on Innovative Areas 23111004 and 23110517 from the Japan Society for the Promotion of Science (Y.U.), and the Ministry of Education, Culture, Sports, Science and Technology, Japan-supported Program for the Strategic Research Foundation at Private Universities (Y.U.).

Disclosures: None declared.

http://dx.doi.org/10.1016/j.ajpath.2015.02.015

the presence of cognitive impairment in these patients, the neuropathological findings have not been investigated. Recently, we reported an autopsy case of genetically confirmed Danon disease and found distinct neuropathological changes, including features of lysosomal accumulation and senescence,[5] although the role of LAMP-2 in the central nervous system (CNS) is still under investigation.

The lysosomal membrane glycoproteins, LAMP-1 and LAMP-2, are type 1 membrane proteins that consist of a short cytoplasmic tail, one transmembrane domain, and a heavily glycosylated luminal domain.[6] Human LAMP-1 and LAMP-2 share 36.7% sequence identity and many structural and biochemical similarities.[7] The human *LAMP2* gene has three splice variants: *LAMP-2A*, *LAMP-2B,* and *LAMP-2C*.[6] LAMP-2A serves as a receptor for chaperone-mediated autophagy (CMA),[8] and CMA malfunction may be related to aging and lysosomal storage diseases, as well as neurodegenerative disorders such as Parkinson disease, Alzheimer disease, and polyglutamine disorders.[9] Fujiwara et al[10,11] discovered a novel function of LAMP-2C that mediates selective autophagy for nucleic acids. Despite the advancement of this field, results from relatively few studies confirm these functions of LAMP-2 *in vivo*.

Here, we examined the CNS of *Lamp-2*–deficient mice. All genes for *Lamp2* subtypes of the mice were deleted.[12] The neuropathological features were consistent with those of human Danon disease,[5] suggesting that *Lamp-2*–deficient mice are an appropriate *in vivo* model for human Danon disease and are, therefore, available to elucidate the mechanism and therapeutic intervention of the disease. Characteristic features, ie, accumulation of glycogen in lysosomes and enhancement of macroautophagy, are not noted in the brain. Different responses between neural cells of the CNS and parenchymal cells of visceral organs are discussed.

Materials and Methods

Experimental Animals

Littermates of male *Lamp2*-deficient mice and wild-type mice were used in this experiment. All of the animals were offspring from pairs of wild-type C57BL/6J male mice and hemizygote $Lamp2^{x/-}$ female mice because the *Lamp2* gene is located at X chromosome Xq24.[13] *Lamp-2*–deficient mice were provided by Dr. Paul Saftig[12] and were backcrossed with C57BL/6J mice >20 generations in our laboratory. The mice were maintained at Juntendo University and at the National Institute of Neuroscience, National Center of Neurology and Psychiatry (Tokyo, Japan). The experiments were approved by the institute's Animal Investigation Committee.

Antibodies

The following primary antibodies were used for Western blot analysis and immunohistochemical analysis: Lamp-2 (M3/84, rat monoclonal, 1:100, Abcam, Cambridge, UK), Lamp-1 (1D4B, rat monoclonal, 1:1000, Stressgen Bioreagents, Victoria, BC, Canada), cathepsin D (rabbit polyclonal, 1:1000, Dr. Yasuo Uchiyama), light chain 3 (LC3) (rabbit polyclonal, 1:1000, Abcam), α-synuclein (rabbit polyclonal, 1:1000 for Western blot analysis, 1:500 for immunohistochemical analysis, EMD Millipore, Billerica, MA), β-actin (mouse monoclonal, 1:10,000, Sigma-Aldrich, St. Louis, MO), ubiquitin (rabbit polyclonal, 1:200, Dako, Glostrup, Denmark), glial fibrillary acidic protein (rabbit polyclonal, 1:1000, Neomarkers, Fremont, CA), Mac-2 (rat monoclonal, 1:500, Cedarlane, Burlington, ON, Canada), GM130 (mouse monoclonal, 1:100, BD, Franklin Lakes, NJ), Rab7 (rabbit polyclonal, 1:100, Santa Cruz Biotechnology, Dallas, TX), microtubule-associated protein 2 (HM2, mouse monoclonal, 1:500, Sigma-Aldrich), ionized calcium-binding adapter molecule 1 (rabbit polyclonal, 1:200, Wako Pure Chemical Industries, Osaka, Japan), 2′,3′-cyclic-nucleotide 3′-phosphodiesterase (mouse monoclonal, 1:200, Covance, Princeton, NJ), SMI31 (mouse monoclonal, 1:1000, Covance), synaptophysin (mouse monoclonal, EMD Millipore), and 4 hydroxynonenal (mouse monoclonal, 1:200, Nikken Seil, Shizuoka, Japan).

Western Blot Analysis

Mice of both genotypes at the age of 12 weeks were deeply anesthetized with diethyl ether and decapitated, and then each tissue was dissected and lysed in radioimmunoprecipitation assay buffer [50 mmol/L Tris-HCl, pH 7.6; 150 mmol/L NaCl; 1% Triton X-100 (Nacalai Tesque, Kyoto, Japan); 0.5% sodium deoxycholate; 0.1% SDS] containing protease inhibitor cocktail (Nacalai Tesque) by means of a homogenizer (Polytron PT3100, Kinematica, Littau-Lucerne, Switzerland). After centrifuging at 10,500 × *g* for 10 minutes at 4°C, the protein concentration of the supernatants was determined by means of a microplate reader SpectraMax M2 (Molecular Devices Japan, Tokyo, Japan) by using bovine serum albumin as a standard. Proteins were separated on 10% or 15% SDS-polyacrylamide gels, transferred to polyvinylidene difluoride membranes (EMD Millipore), and incubated with 5% skim milk in phosphate-buffered saline (PBS) with Tween 20 [135 mmol/L PBS containing 0.05% Tween 20 (Nacalai Tesque)] for 1 hour at room temperature. The membranes were incubated overnight with each primary antibody, washed in PBS with Tween 20, and further incubated with anti-mouse or rabbit IgG horseradish peroxidase conjugate (1:1000, Dako). After washing in PBS with Tween 20, the membranes were developed with chemiluminescent horseradish peroxidase substrate (Immobilon Western, EMD Millipore) and analyzed using the LAS-4000 luminescent image analyzer (Fujifilm, Tokyo, Japan). β-Actin was used as a loading control. Statistical analyses ($n = 3$) were performed using a Student's *t*-test in Excel (Microsoft, Redmond, WA).

Immunohistochemical Analysis

For immunohistochemical studies, male mice of both genotypes at 12 and 32 weeks of age (total 12 mice) were deeply anesthetized with diethyl ether and perfused with 4% paraformaldehyde. The brain, heart, and liver were removed and postfixed overnight and then embedded in paraffin and sectioned. Sections (5 μm thick) were deparaffinized and treated with 1% hydrogen peroxide for 30 minutes, autoclaved at 105°C for 10 minutes, and then incubated with 5% normal serum in PBS (pH 7.4) for 1 hour at room temperature followed by incubation overnight at 4°C with each primary antibody. The sections were washed in PBS then incubated with biotinylated secondary antibodies diluted 1:500 in PBS containing 5% normal serum. The sections were treated with the VECTASTAIN Elite ABC kit (Vector Laboratories, Burlingame, CA) according to the manufacturer's protocol. Some sections were incubated with EnVision + System horseradish peroxidase—labeled polymer anti-rabbit or anti-mouse (Dako) as secondary antibodies. Sections were developed with 0.02% 3,3′-diaminobenzidine tetrahydrochloride solution containing 0.003% hydrogen peroxide. After visualization, sections were counterstained with hematoxylin.

For single or double immunofluorescent studies, sections were incubated with primary antibodies overnight, followed by secondary antibodies conjugated to Alexa Fluor 488 and/or 594 (1:200, Molecular Probes, Thermo Fisher Scientific, Eugene, OR) for 1 hour, then DAPI (250 nmol/L) for 5 minutes. Confocal microscopy was performed using the FluoView FV1000 confocal microscope system (Olympus, Tokyo, Japan). The percentage of intracellular particles that were immunoreactive for Lamp-2, Lamp-1, or Rab7 was counted in 100 particles of hippocampal large neurons for three candidates from each wild-type and *Lamp-2*—deficient mice groups.

Fluorescein Isothiocyanate Lectin Staining for Glycoanalysis

To identify the profiling of glycans for intracytoplasmic aggregates, we stained fluorescein isothiocyanate—conjugated lectins. Paraffin-embedded 4% paraformaldehyde-fixed sections were deparaffinized and incubated with 3% bovine serum albumin in PBSfor 1 hour at room temperature followed by incubation overnight at 4°C with each fluorescein isothiocyanate—conjugated lectin for concanavalin A, succinyl concanavalin A, wheat germ agglutinin, *Lens culinaris* agglutinin, *Psathyrella velutina* lectin, *Phaseolus vulgaris* erythrolectin, *Vicia villosa* lectin, *Galanthus nivalis* lectin, or *Bauhinia purpurea* lectin (Sigma-Aldrich) diluted 1:500 in 3% bovine serum albumin in PBS. The sections were observed with a confocal laser scanning microscope (FluoView FV1000, Olympus).

Electron Microscopic Analysis

Both genotypes of male mice at the age of 8 and 34 weeks (total eight mice) were deeply anesthetized with dimethyl ether and perfused with 2% paraformaldehyde and 2% glutaraldehyde in 0.1 mol/L phosphate buffer (pH 7.4). The brain and liver were removed, postfixed with the same fixative, and left overnight at 4°C. The specimens were trimmed and washed with PBS, incubated in phosphate-buffered 1% osmium tetroxide for 1 hour, dehydrated in ethanol, and embedded in resin (Epon 812, TAAB Laboratories Equipment, Berkshire, UK). Ultrathin sections were mounted on copper grids and stained with uranyl acetate and lead citrate. The sections were observed using an H-7000 electron microscope (Hitachi, Tokyo, Japan) or Tecnai transmission electron microscope (FEI, Hillsboro, OR).

Results

General Appearance of *Lamp-2*—Deficient Mice

The body weights of *Lamp-2*—deficient mice were significantly reduced when compared with those of wild-type mice at 16 weeks of age (Supplemental Figure S1). *Lamp-2*—deficient mice are reported to have increased mortality between 20 and 40 days of age.[12] In our observation, life spans of the mice that survived >40 days were also shortened (Supplemental Figure S2).

Localization of Lamp-2 in the CNS

Lamp-2 protein is abundant in the liver, and to a lesser extent, in the heart and brain of wild-type mice at the age of 12 weeks (Figure 1A). Expression of Lamp-2 was lacking in the *Lamp-2*—deficient mice (Figure 1, A—E). Double immunohistochemical analysis revealed that immunoreactivity for Lamp-2 largely colocalized in granules with immunoreactivity for Lamp-1 (89.3%), and some granules immunopositive for Lamp-2 colocalized with those for a late endosome marker, Rab7 (10.7%) (Figure 1, F and G). In the CNS, Lamp-2 was expressed ubiquitously in the neurons (microtubule-associated protein 2) (Figure 1, H—J), astrocytes (glial fibrillary acidic protein) (Figure 1, K—M), microglia (ionized calcium-binding adapter molecule 1) (Figure 1, N—P), and oligodendrocytes (2′,3′-cyclic-nucleotide 3′-phosphodiesterase) (Figure 1, Q—S), showing relatively prominent staining in large neurons (Figure 1D).

Morphological and Functional Changes in Lysosomes in *Lamp-2*—Deficient Mice

To study the structural and immunohistochemical changes in lysosomes, expression of another lysosomal membrane protein, Lamp-1 and a lysosomal aspartic proteinase, we examined cathepsin D. Western blot analysis showed that expression of Lamp-1 and cathepsin D was significantly increased in the brain of *Lamp-2*—deficient mice (Figure 2, A and B). Both Lamp-1 and cathepsin D—immunoreactive lysosomes were enlarged, especially in the large neurons of *Lamp-2*—deficient mice (Figure 2, C—H).

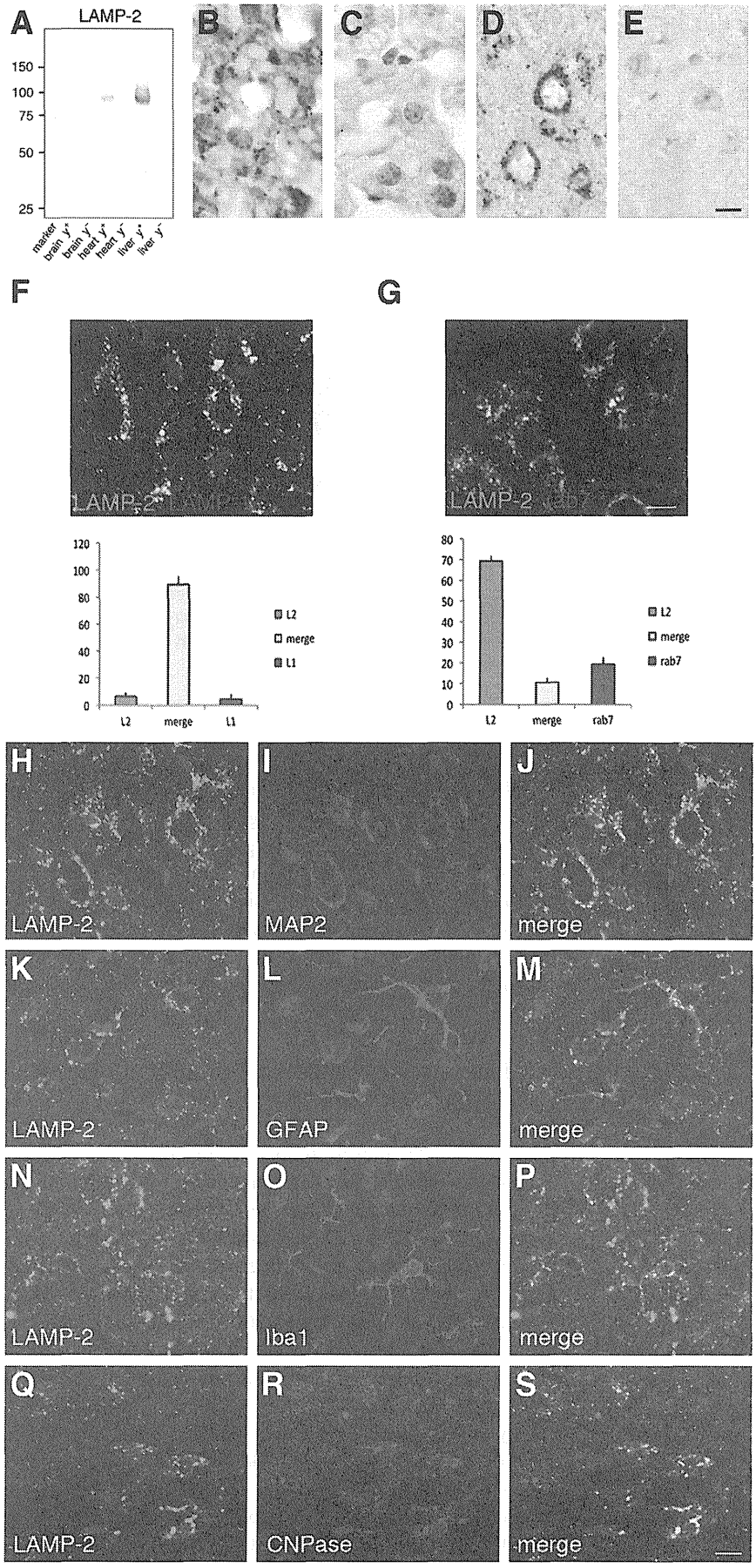

Figure 1 Lysosome-associated membrane protein-2 (Lamp-2) is expressed mainly in the lysosomes and enriched in the large neurons of the brain. **A:** Western blot analysis of Lamp-2 with lysates from the brain (30 μg per lane), heart (10 μg per lane), and liver (10 μg per lane) in wild-type and *Lamp-2*—deficient mice. The immunoreactive band for Lamp-2 is undetectable in *Lamp-2*—deficient mice. **B—E:** Immunoreactivity for Lamp-2 is observed in the liver (**B**) and neocortex (**D**) of the wild-type mice, whereas little immunoreactivity is seen in the liver (**C**) and neocortex (**E**) of the *Lamp-2*—deficient mice. **F** and **G:** Double immunohistochemical analysis reveals that Lamp-2 colocalizes with Lamp-1 (**F**; 89.3%) and with Rab7 (**G**; 10.7%). **H—S:** Lamp-2 partially colocalizes with microtubule-associated protein 2 (MAP2; **H—J**), glial fibrillary acidic protein (GFAP; **K—M**), ionized calcium-binding adapter molecule 1 (Iba1; **N—P**), and 2′,3′-cyclic-nucleotide 3′-phosphodiesterase (CNPase; **Q—S**). Scale bars: 10 μm.

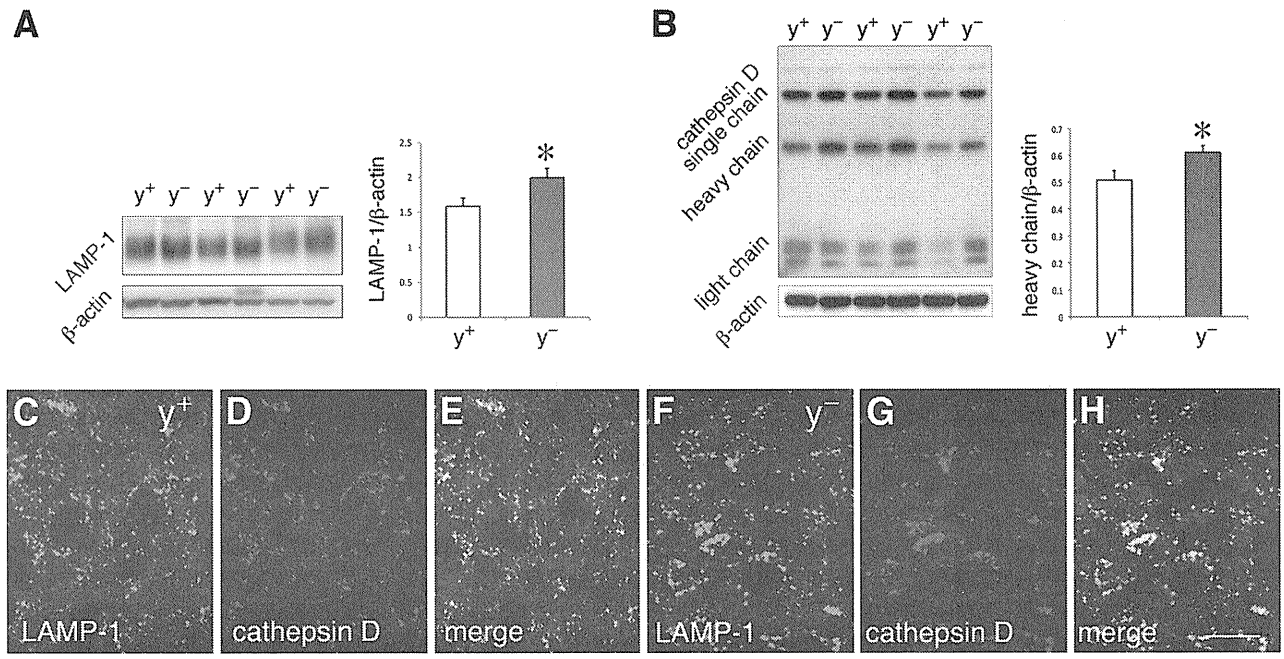

Figure 2 Expression of lysosome-associated membrane protein-2 (Lamp-1) and cathepsin D increases in the brain of *Lamp-2*—deficient mice. **A** and **B:** Western blot analysis reveals that expression of both Lamp-1 (**A**) and cathepsin D (**B**) significantly increases in the brain of *Lamp-2*—deficient mice (y^-) compared with in wild-type mice (y^+). Each value represents the means ± SEM. **C—H:** Double immunohistochemical analysis shows Lamp-1 and cathepsin D—immunoreactive lysosomes are enlarged in the CA3 of *Lamp-2*—deficient mice (12 weeks **F—H**). $*P < 0.05$. Scale bar = 10 μm.

Electron microscopic observations showed primary lysosomes in wild-type mice (Figure 3, A and D) and accumulation of glycogen granules and membranous materials in lysosomes of the liver in *Lamp-2*—deficient mice at the age of 8 weeks (Figure 3, B and C). Although morphological changes in lysosomes were also observed in the hippocampal neurons of *Lamp-2*—deficient mice, glycogen granules did not accumulate in lysosomes (Figure 3, E and F). Lipofuscin in the large neurons was sometimes seen in the 34-week-old wild-type mice (Figure 3G). In addition to lipofuscin, vesicle-containing structures were seen in the cytoplasm of hippocampal neurons in *Lamp-2*—deficient mice (Figure 3H). Various materials accumulated not only in neurons but also in other cell types in the CNS of *Lamp-2*-deficient mice. Aggregates of membrane structures were detected in astrocytes (Figure 3I), whereas electron-dense materials packed in large granules that contained small electron-dense and -lucent vesicles were present in pericytes (Figure 3J).

To identify the properties of lysosomal accumulation, we performed immunohistochemical analysis for ubiquitin (Figure 4, A—D) and lectin staining (Figure 4, E and F). Ubiquitin-immunoreactive aggregates were found in the neuronal perikarya of the neocortex and hippocampal CA3 region (Figure 4, B and D). At confocal laser scanning microscopy, autofluorescence was detected in granular structures, some of which colocalized with positive staining for concanavalin A that interacts with D-mannose and D-glucose; these appeared more abundantly in the hippocampal CA3 neurons of *Lamp-2*—deficient mice than in those of wild-type mice (Figure 4, E and F).

Alterations of the Golgi Apparatus in Large Neurons

Besides morphological and functional changes in lysosomes, the structure of the Golgi apparatus was altered in the *Lamp-2*—deficient mice (Figure 5). Immunoreactivity for GM130, a Golgi matrix protein, increased in large neurons of *Lamp-2*—deficient mice at the age of 12 weeks (Figure 5, A and B). Ultrastructurally, the cisternae of the Golgi lamellae were dilated at the age of 8 weeks, and some cisternae took a circular form at the age of 32 weeks (Figure 5, C—F).

Cell-Type Specific Changes in Expression for LC3 in *Lamp-2*—Deficient Mice

Because skeletal muscle biopsy results for Danon disease exhibit autophagic vacuolar myopathy,[3,4] expression of LC3, a macroautophagy marker protein, was examined. Expression levels of LC3-II, a membrane-bound type, were significantly increased in the liver of the *Lamp-2*—deficient mice compared with that in control mice, as evidenced by Western blot analysis (Figure 6A) ($P < 0.05$), whereas expression levels of LC3-II were similar in the brain of both phenotypes (Figure 6B). Immunoreactivity for LC3 was detected in large granules in the cardiac myocytes and hepatocytes of *Lamp-2*—deficient mice (Figure 6, C—F). Electron micrographs showed a large amount of autophagic vacuoles and dense bodies in the liver of *Lamp-2*—deficient mice (Figure 6G). In the brain, expression of LC3 in *Lamp-2*—deficient mice was similar to that in wild-type mice

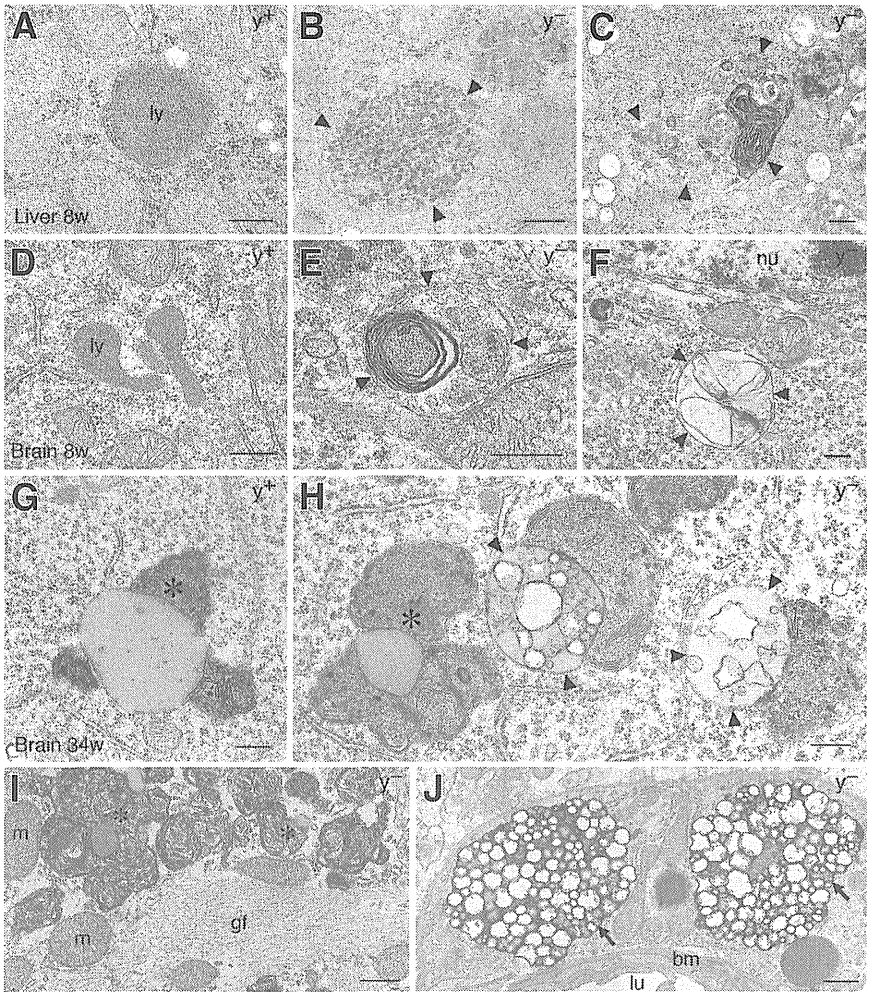

Figure 3 Ultrastructure of lysosomes and accumulation of various materials in the liver at 8 weeks (w) (**A**–**C**) and brain at 8 weeks (**D**–**F**) and 34 weeks (**G**–**J**) in wild-type mice (y^+; **A, D,** and **G**) and *Lamp-2*–deficient mice (y^-; **B, C, E, F,** and **H**–**J**). **A**–**C:** Lysosomes (ly) appear as electron-dense organelles in the liver of wild-type mice. Accumulations of glycogen (**arrowheads, B**) and membranous materials (**arrowheads, C**) in lysosomes are observed in the liver of *Lamp-2*–deficient mice. **D**–**F:** In contrast to lysosomes in neuronal cytoplasm of 8-week-old wild-type mice, lysosomal changes with membranous accumulations are found in the neurons of *Lamp-2*–deficient mice (**arrowheads, E** and **F**). **G**–**J:** In the brain at the age of 34 weeks, lipofuscin is observed in hippocampal CA3 neurons of both wild-type and *Lamp-2*–deficient mice (**asterisk, G** and **H**). In addition, vesicle-containing materials (**arrowheads, H**) are seen in the cytoplasm of neurons in *Lamp-2*–deficient mice. Membranous materials in astrocytes (**asterisks, I**) and electron-dense materials with small vesicles in pericytes (**arrows, J**) are also accumulated. bm, basement membrane; gf, glial filaments; lu, lumen; m, mitochondria; nu, nucleus. Scale bars: 250 nm (**A**–**H**); 500 nm (**I** and **J**).

(Figure 6, H and I) except for in the substantia nigra pars reticulata, where some LC3-immunoreactive large granular structures (Figure 6, J and K) and autophagic vacuole–containing axons were observed (Figure 6L). Although Western blot analysis for LC3-II with use of whole brain lysates did not show any difference between wild-type and *Lamp-2*–deficient mice (Figure 6B), analysis with midbrain lysates revealed increased expression of LC3-II in *Lamp-2*–deficient mice (Supplemental Figure S3A). Irrespective of such findings in the substantia nigra, neuronal loss of dopaminergic neurons was not observed with tyrosine hydroxylase staining (data not shown).

Midbrain Pathology with Extensive Glial Reactions

To further investigate the midbrain pathology, we performed immunohistochemical analysis for α-synuclein, one of the most important CMA substrates, and relevant proteins (Figure 7). First, we confirmed that the antibody for α-synuclein would not cross-react with β- or γ-synuclein (data not shown). Although expression of α-synuclein (Figure 7M) and a key regulator for CMA, Hsc70 (Supplemental Figure S3B), in the brain of *Lamp-2*–deficient mice was similar to that of wild-type mice, immunohistochemical studies revealed that large dotted structures positive for α-synuclein were found in the substantia nigra pars reticulata (Figure 7, A–D). Expression of α-synuclein in the dotted structures was not seen after proteinase K treatment (Supplemental Figure S4). Phosphorylated α-synuclein was not detected in the *Lamp-2*–deficient brain (data not shown). The structures were colocalized in part with SMI31, synaptophysin, Mac-2, and 4 hydroxynonenal (Figure 7, N–Q), suggesting that axons and activated microglia are associated with lipid peroxidation. In the substantia nigra, extensive reactive astrocytosis (Figure 7, E–H) and activated microglial infiltration (Figure 7, I–L) were observed.

Discussion

Expression of Lamps in the CNS

LAMPs are major components of lysosome membranes. In our observation, Lamp-2 was ubiquitously distributed to different cell types and enriched in the large neurons in the CNS. The majority of Lamp-2–immunoreactive vesicles colocalized with Lamp-1 in these large neurons. Although

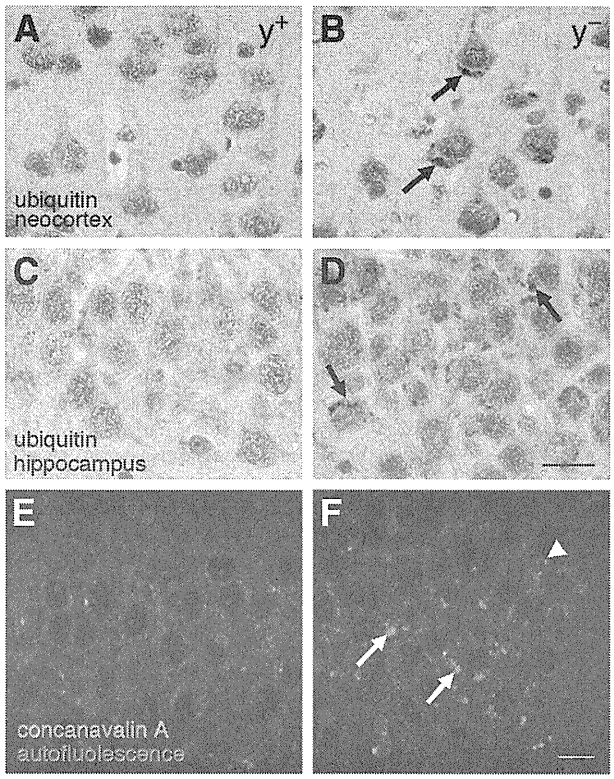

Figure 4 Expression of ubiquitin and concanavalin A increases in the large neurons of *Lamp-2*—deficient mice at the age of 32 weeks. **A—D:** Immunohistochemical images for ubiquitin in the neocortex (**A** and **B**) and hippocampal CA3 (**C** and **D**) in wild-type (y^+; **A** and **C**) and *Lamp-2*—deficient (y^-; **B** and **D**) mice reveals that large neurons in *Lamp-2*—deficient mice contain ubiquitin-immunoreactive aggregates (**arrows**, **B** and **D**). **E** and **F:** Concanavalin A staining (green; **arrows**, **F**) and autofluorescence (red; **arrowhead**, **F**) positive deposits in the hippocampal CA3 are abundant in *Lamp-2*—deficient mice (**F**) compared with those in wild-type mice (**E**). Scale bar = 20 μm.

Lamp-1—deficient mice exhibited mild gliosis and altered cathepsin D immunoreactivity in the brain with normal lysosomal morphology,[14] double deficiency of both Lamp-1 and Lamp-2 is embryonic lethal.[15] Because expression of Lamp-1 was elevated in the brains of *Lamp-2*—deficient mice, it is likely that these two proteins are interdependent in CNS neurons. Therefore, phenotypes of *Lamp-2*—deficient mice may indicate a specific function for Lamp-2.

Lamp-2—Deficient Mice as a Model of Lysosomal Storage Disease

Two-thirds of lysosomal storage diseases involve the CNS; however, their exact contribution to mental retardation remains unknown.[16] *LAMP-2*—deficient human Danon disease was first diagnosed as a glycogen storage disease because glycogen granules accumulated in the muscle.[2] We observed accumulations of electron-dense materials and ubiquitin-immunoreactive aggregates in the neuronal cytoplasm of the *Lamp-2*—deficient brain. Because various shaped materials accumulated in the different cell types of *Lamp-2*—deficient mice, these findings are likely not the consequence of deficiency of a single lysosomal enzyme but a disorder of enzyme trafficking or targeting or defective function of nonenzymatic lysosomal proteins. Results from functional studies have revealed that LAMP-2 deficiency leads to impaired recycling of 46-kDa mannose 6-phosphate receptors and partial mistargeting of lysosomal enzyme.[17] LAMP-2 also plays a critical role in endosomal cholesterol transport.[18] Our morphological studies are consistent with those in these reports.

Lectin staining revealed that intracellular aggregates were positive for concanavalin A, which binds D-mannose and

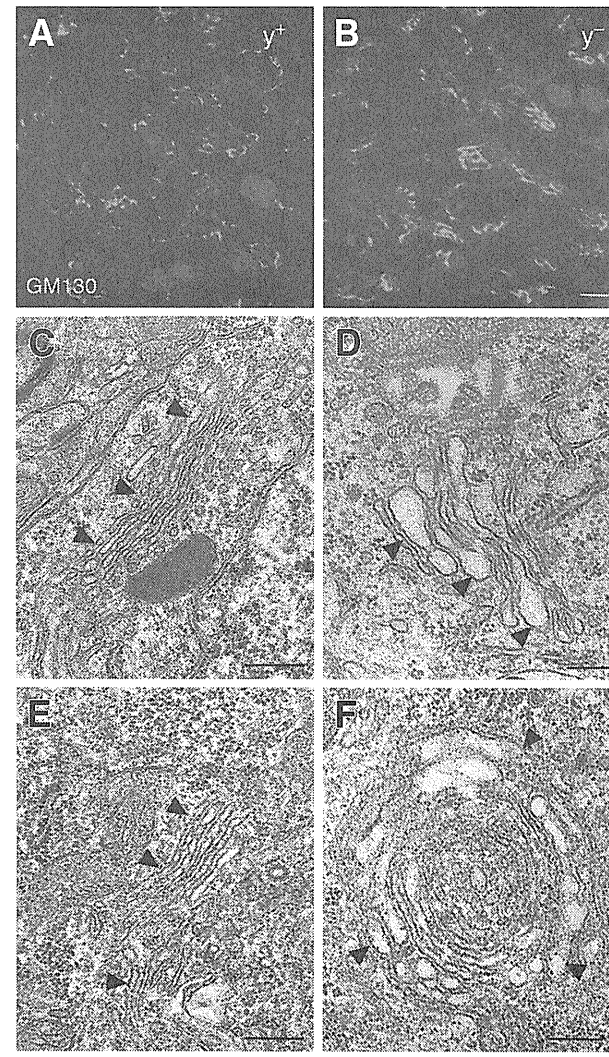

Figure 5 Structure of Golgi apparatus is altered in the neurons of *Lamp-2*—deficient mice. **A** and **B:** Immunoreactivity for GM130 is more abundant in the hippocampal pyramidal neurons of *Lamp-2*—deficient mice (y^-) than that in wild-type mice (y^+). **C—F:** Electron micrographs show that the Golgi apparatus appears as thin lamellar structures in the CA3 neurons of wild-type mice (8 weeks, **C**; 32 weeks, **E**; indicated by **arrowheads**). In the neurons of *Lamp-2*—deficient mice, dilatation of cisternae (8 weeks, **D**; indicated by **arrowheads**) and circular structures (32 weeks, **F**; indicated by **arrowheads**) are observed. Scale bars: 10 μm (**A** and **B**); 250 nm (**C—F**).

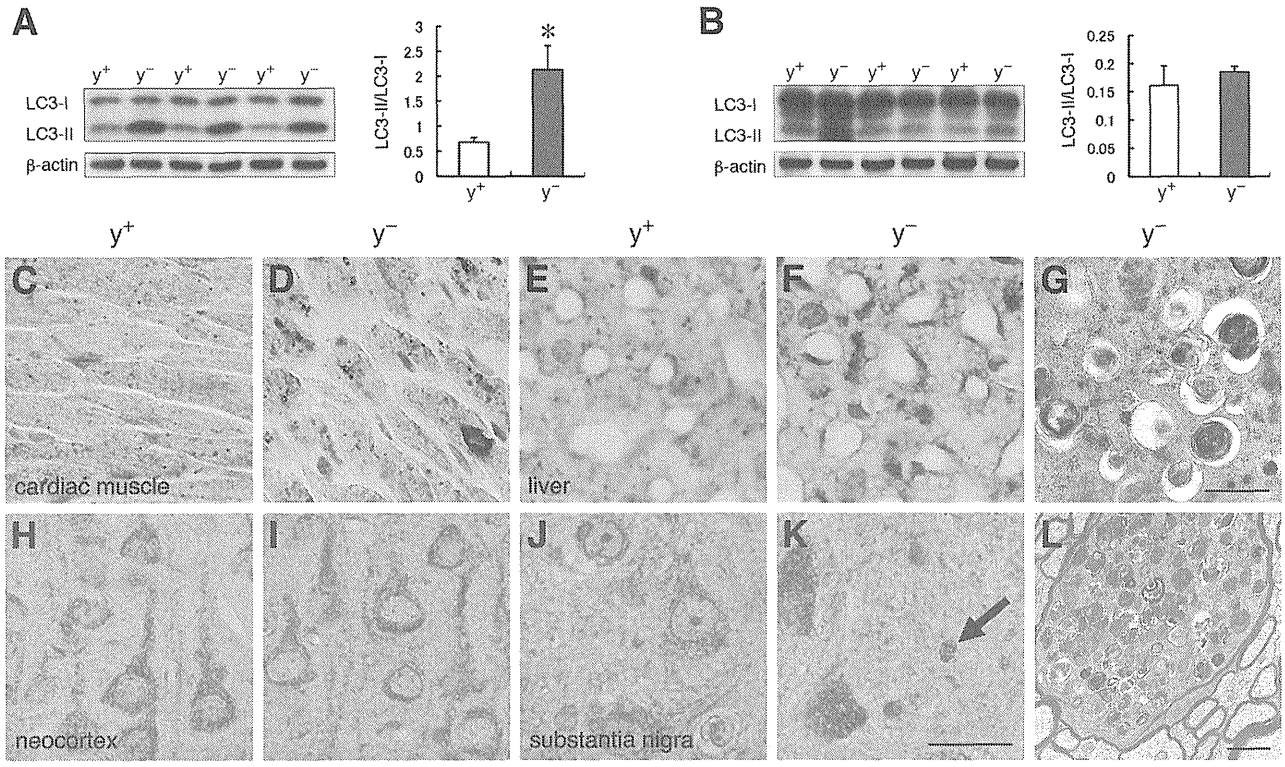

Figure 6 Macroautophagy is less affected in the brain of *Lamp-2*—deficient mice at the age of 12 weeks. **A** and **B:** Western blot analysis reveals that expression of membrane-bound type light chain 3 (LC3)-II significantly increases in the liver of *Lamp-2*—deficient mice (**A**); however, there is no significant change of LC3 expression in the central nervous system (CNS) (**B**). β-Actin was used as a loading control. **C**—**F** and **H**—**K:** Immunohistochemical analysis for LC3 in the cardiac muscle (**C** and **D**), liver (**E** and **F**), cerebral neocortex (**H** and **I**), and substantia nigra (**J** and **K**) of wild-type mice (y^+) and *Lamp-2*—deficient mice (y^-). In the *Lamp-2*—deficient mice, LC3-immunoreactive deposits are found in cardiac muscle (**D**) and hepatocytes (**F**); however, such immunoreactivity is not found in the CNS (**I** and **K**), except for LC3-positive large granular structures in the substantia nigra pars reticulata (**arrow, K**). **G** and **L:** Electron micrographs show accumulations of autophagic vacuoles and dense bodies in the hepatocytes (**G**) and axons of the substantia nigra (**L**) in *Lamp-2*—deficient mice. Each value represents the means ± SEM. $*P < 0.05$. Scale bars: 20 μm (**C**—**F, H**—**K**); 500 nm (**G**); 1 μm (**L**).

D-glucose. Virtanen et al[19] examined storage material in cultured fibroblasts by specific lectin binding in several lysosomal storage diseases and found that concanavalin A was positive for the materials in I-cell disease, which is a deficiency of phosphotransferase in the Golgi apparatus. In addition to the lysosomal changes, dysfunction of intracellular organelles, including the mitochondria, endoplasmic reticulum, and Golgi apparatus, has been described in lysosomal storage diseases.[16] Large neurons of *Lamp-2*—deficient mice showed increased immunoreactivity for GM130 and morphological changes in the cisternae of Golgi lamellae. Accumulation of GM130 leads to alterations of Golgi ribbon architecture.[20] Collectively, these findings in the CNS, in addition to growth retardation and low survival rate beyond postnatal day 40 (Supplemental Figures S1 and S2), are consistent with those of lysosomal storage disease. The main neuropathological feature—accumulation of lysosomes—is similar to that in human Danon disease.[5]

Region-Specific Differences in Macroautophagy

A large amount of autophagic vacuoles were found in the parenchymal cells of the various visceral organs both in Danon disease and *Lamp-2*—deficient mice.[1,12] Moreover, in the present study, we confirmed the elevation of autophagic activity in the heart and liver of *Lamp-2*—deficient mice. Multiple functions of LAMPs have been suggested so far: cholesterol traffic,[15] fusion of lysosomes with phagosomes,[21] and major histocompatibility complex class II antigen presentation.[22] Expression of LAMP-2 is also related to pathological processes such as neoplasms and inflammation,[23–25] although few experimental data on LAMP-2 have been shown in neuronal cells.

In the CNS, autophagic vacuoles were not observed in neurons except for some axons in the substantia nigra. Such cell-type specific alterations in the *Lamp-2*—deficient mice suggest that Lamp-2 may have distinct functions in each tissue or cell type. Constitutive autophagy is important in the CNS because lack of autophagy-related protein 7 or autophagy-related protein 5 in CNS tissue causes neuronal changes with ubiquitin-positive inclusion bodies.[26,27] It is uncertain why neurons do not show many autophagic vacuoles in the *Lamp-2*—deficient brains. Neurons may have protective mechanisms against excessive autophagic processes. Another possible mechanism may be that Lamp-2 has no effects on autophagosomes in neurons.

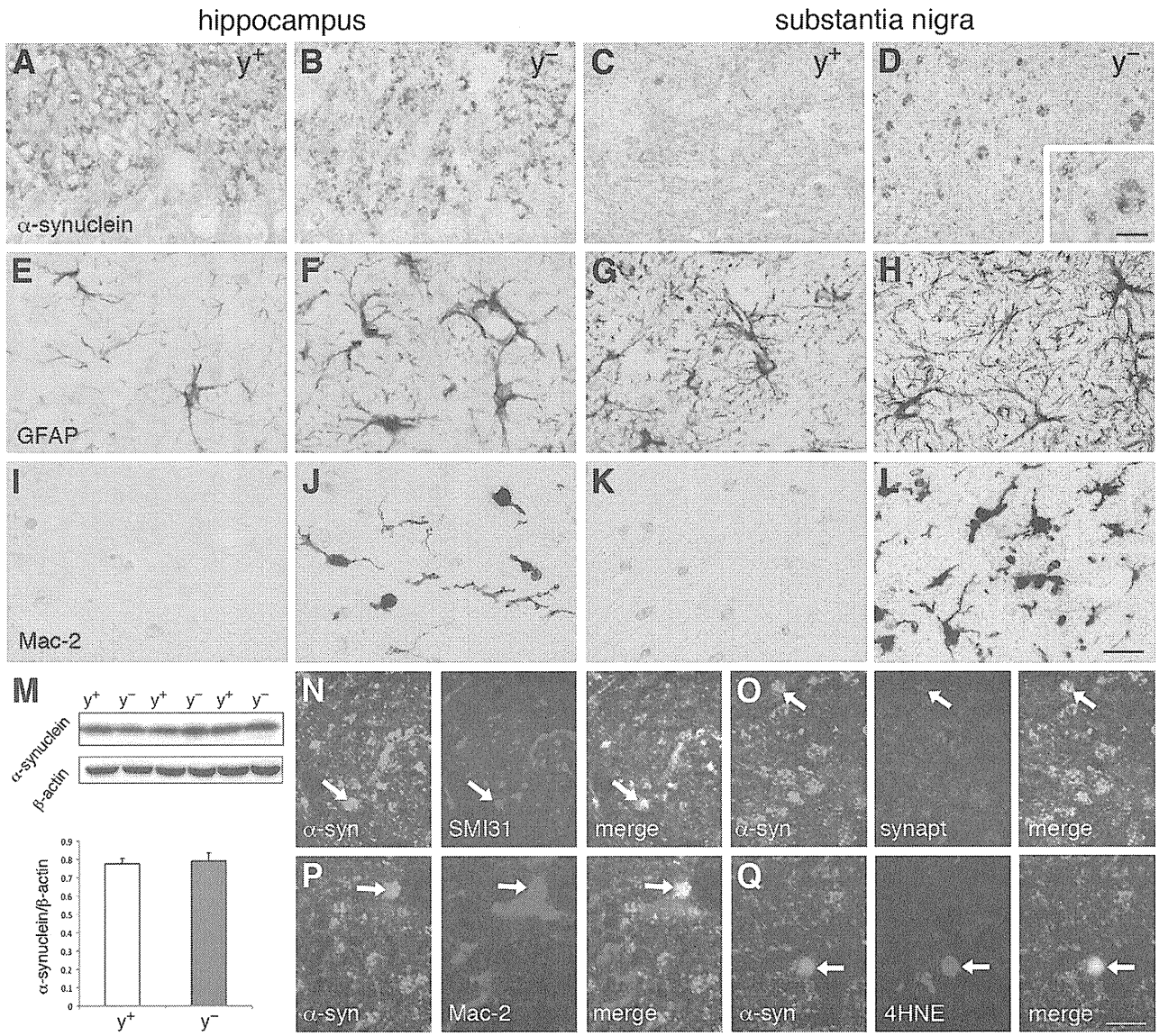

Figure 7 α-Synuclein—immunoreactive structures with extensive glial changes and oxidative stress are seen in the substantia nigra at the age of 12 weeks. **A—L:** Immunohistochemical analysis for α-synuclein (**A—D**), glial fibrillary acidic protein (GFAP; **E—H**), and Mac-2 (**I—L**) in the hippocampus (**A, B, E, F, I,** and **J**) and substantia nigra (**C, D, G, H, K,** and **L**). α-Synuclein—immunoreactive structures are found in the substantia nigra (**D; inset, D**). Extensive infiltration of GFAP-positive reactive astrocytes (**F** and **H**) and Mac-2-positive activated microglia (**J** and **L**) are seen in the substantia nigra and to a lesser extent in the hippocampus of *Lamp-2*—deficient mice. **M:** Western blot analysis for α-synuclein in the brain shows no significant changes between wild-type and *Lamp-2*—deficient mice. β-Actin is used as a loading control. **N—Q:** Double immunofluorescence for α-synuclein (α-syn; green) and SMI31 (**N**, red), synaptophysin (synapt; **O**, red), Mac-2 (**P**, red), and 4 hydroxynonenal (4HNE; **Q**, red) reveals colocalization of α-synuclein and each protein (**N—Q, arrows**). Scale bars: 20 μm (**A—L**); 10 μm (**inset, D**, and **N—Q**).

Evidence of Midbrain Pathology Associated with Excessive Glial Reactions and Lipid Peroxidation

We found intense astrocytic and microglial reactions in the substantia nigra and hippocampus of *Lamp-2*—deficient mice. Glial cells are also involved primarily in lysosomal storage diseases.[28] Accumulation of membranous materials was found in the astrocytes of *Lamp-2*—deficient mice (Figure 3I). Relationships between lysosomal disease and Parkinson disease, as well as oxidative stress, have been suggested.[29,30] Lysosomal dysfunction owing to LAMP-2 deficiency may cause lipid peroxidation, which enhances midbrain pathology; however, in *Lamp-2*—deficient mice, proteinase K—resistant α-synuclein did not accumulate, and a loss of dopaminergic neurons was not obvious.

Selective Degradation in the Lysosomes via Lamp-2 Subtypes

α-Synuclein is one of the most important substrates for CMA, and impaired degradation has been implicated in Parkinson disease.[31] Although some axonal swelling and

activated microglial cells were immunoreactive for α-synuclein, Western blot analysis for α-synuclein with whole brain or midbrain homogenates did not show any difference between wild-type and *Lamp-2*–deficient mice. Moreover, phosphorylated α-synuclein was not expressed in *Lamp-2*–deficient brains. Glyceraldehyde-3-phosphate dehydrogenase, another CMA substrate, also did not increase in *Lamp-2*–deficient mice.[10] CMA is activated during oxidative stress,[32] and protein degradation *in vivo* has an alternative pathway; eg, α-synuclein is also degraded by macroautophagy, the ubiquitin-proteasome system,[33] and other proteases such as calpains, neurosin, and metalloproteinases.[34] Although glyceraldehyde-3-phosphate dehydrogenase is known as a CMA substrate, 4 hydroxynonenal–modified glyceraldehyde-3-phosphate dehydrogenase could also be degraded by cathepsin G.[35] Therefore, a decrease in CMA activity owing to Lamp-2 deficiency could be compensated for by constitutive autophagy or the ubiquitin-proteasome system in the CNS of *Lamp-2*–deficient mice. Another possible explanation may be that unknown receptors are involved in CMA. LAMP-2C is mainly expressed in neurons in the CNS and mediates RNautophagy and DNautophagy.[10,11] Degradation of nucleic acids, in particular RNA, may be important in maintaining the neuronal environment. Another subtype, LAMP-2B is enriched in the liver and skeletal muscle. Because a patient with a frameshift of exon 9b shows full symptoms of Danon disease, including mental retardation, the function of LAMP-2B is crucial for Danon disease,[1] although the role of LAMP-2B in the CNS is unknown. Further investigation is required for understanding the specific function of each LAMP-2 subtype *in vivo*.

Acknowledgments

We thank Drs. Kiyomitsu Oyanagi, Kinuko Suzuki, and Koh Furuta for useful discussions, Drs. Paul Saftig and Judith Blanz for providing *Lamp-2*–deficient mice, Chihana Kabuta, Yohei Fujimoto, and Osamu Aizawa for technical assistance, and Robert Debold for editing the manuscript.

Supplemental Data

Supplemental material for this article can be found at *http://dx.doi.org/10.1016/j.ajpath.2015.02.015*.

References

1. Nishino I, Fu J, Tanji K, Yamada T, Shimojo S, Koori T, Mora M, Riggs JE, Oh SJ, Koga Y, Sue CM, Yamamoto A, Murakami N, Shanske S, Byrne E, Bonilla E, Nonaka I, DiMauro S, Hirano M: Primary LAMP-2 deficiency causes X-linked vacuolar cardiomyopathy and myopathy (Danon disease). Nature 2000, 406:906–910
2. Danon MJ, Oh SJ, DiMauro S, Manaligod JR, Eastwood A, Naidu S, Schliselfeld LH: Lysosomal glycogen storage disease with normal acid maltase. Neurology 1981, 31:51–57
3. Nishino I: Autophagic vacuolar myopathies. Curr Neurol Neurosci Rep 2003, 3:64–69
4. Sugie K, Noguchi S, Kozuka Y, Arikawa-Hirasawa E, Tanaka M, Yan C, Saftig P, von Figura K, Hirano M, Ueno S, Nonaka I, Nishino I: Autophagic vacuoles with sarcolemmal features delineate Danon disease and related myopathies. J Neuropathol Exp Neurol 2005, 64:513–522
5. Furuta A, Wakabayashi K, Haratake J, Kikuchi H, Kabuta T, Mori F, Tokonami F, Katsumi Y, Tanioka F, Uchiyama Y, Nishino I, Wada K: Lysosomal storage and advanced senescence in the brain of LAMP-2-deficient Danon disease. Acta Neuropathol 2013, 125:459–461
6. Eskelinen EL, Cuervo AM, Taylor MR, Nishino I, Blum JS, Dice JF, Sandoval IV, Lippincott-Schwartz J, August JT, Saftig P: Unifying nomenclature for the isoforms of the lysosomal membrane protein LAMP-2. Traffic 2005, 6:1058–1061
7. Fukuda M, Viitala J, Matteson J, Carlsson SR: Cloning of cDNAs encoding human lysosomal membrane glycoproteins, h-lamp-1 and h-lamp-2. Comparison of their deduced amino acid sequences. J Biol Chem 1988, 263:18920–18928
8. Cuervo AM, Dice JF: A receptor for the selective uptake and degradation of proteins by lysosomes. Science 1996, 273:501–503
9. Koga H, Cuervo AM: Chaperone-mediated autophagy dysfunction in the pathogenesis of neurodegeneration. Neurobiol Dis 2011, 43:29–37
10. Fujiwara Y, Furuta A, Kikuchi H, Aizawa S, Hatanaka Y, Konya C, Uchida K, Yoshimura A, Tamai Y, Wada K, Kabuta T: Discovery of a novel type of autophagy targeting RNA. Autophagy 2013, 9:403–409
11. Fujiwara Y, Kikuchi H, Aizawa S, Furuta A, Hatanaka Y, Konya C, Uchida K, Wada K, Kabuta T: Direct uptake and degradation of DNA by lysosomes. Autophagy 2013, 9:1167–1171
12. Tanaka Y, Guhde G, Suter A, Eskelinen EL, Hartmann D, Lüllmann-Rauch R, Janssen PM, Blanz J, von Figura K, Saftig P: Accumulation of autophagic vacuoles and cardiomyopathy in LAMP-2-deficient mice. Nature 2000, 406:902–906
13. Manoni M, Tribioli C, Lazzari B, DeBellis G, Patrosso C, Pergolizzi R, Pellegrini M, Maestrini E, Rivella S, Vezzoni P, et al: The nucleotide sequence of a CpG island demonstrates the presence of the first exon of the gene encoding the human lysosomal membrane protein lamp2 and assigns the gene to Xq24. Genomics 1991, 9:551–554
14. Andrejewski N, Punnonen EL, Guhde G, Tanaka Y, Lüllmann-Rauch R, Hartmann D, von Figura K, Saftig P: Normal lysosomal morphology and function in LAMP-1-deficient mice. J Biol Chem 1999, 274:12692–12701
15. Eskelinen EL, Schmidt CK, Neu S, Willenborg M, Fuertes G, Salvador N, Tanaka Y, Lüllmann-Rauch R, Hartmann D, Heeren J, von Figura K, Knecht E, Saftig P: Disturbed cholesterol traffic but normal proteolytic function in LAMP-1/LAMP-2 double-deficient fibroblasts. Mol Biol Cell 2004, 15:3132–3145
16. Bellettato CM, Scarpa M: Pathophysiology of neuropathic lysosomal storage disorders. J Inherit Metab Dis 2010, 33:347–362
17. Eskelinen EL, Illert AL, Tanaka Y, Schwarzmann G, Blanz J, von Figura K, Saftig P: Role of LAMP-2 lysosome biogenesis and autophagy. Mol Biol Cell 2002, 13:3355–3368
18. Schneede A, Schmidt CK, Hölttä-Vuori M, Heeren J, Willenborg M, Blanz J, Domanskyy M, Breiden B, Brodesser S, Landgrebe J, Sandhoff K, Ikonen E, Saftig P, Eskelinen EL: Role for LAMP-2 in endosomal cholesterol transport. J Cell Mol Med 2011, 15:280–295
19. Virtanen I, Ekblom P, Laurila P, Nordling S, Raivio KO, Aula P: Characterization of storage material in cultured fibroblasts by specific lectin binding in lysosomal storage diseases. Pediatr Res 1980, 14:1199–1203
20. Roy E, Bruyère J, Flamant P, Bigou S, Ausseil J, Vitry S, Heard JM: GM130 gain-of-function induces cell pathology in a model of lysosomal storage disease. Hum Mol Genet 2012, 21:1481–1495
21. Huynh KK, Eskelinen EL, Scott CC, Malevanets A, Saftig P, Grinstein S: LAMP proteins are required for fusion of lysosomes with phagosomes. EMBO J 2007, 26:313–324
22. Crotzer VL, Glosson N, Zhou D, Nishino I, Blum JS: LAMP-2-deficient human B cells exhibit altered MHC class II presentation of exogenous antigens. Immunology 2010, 131:318–330

23. Furuta K, Ikeda M, Nakayama Y, Nakamura K, Tanaka M, Hamasaki N, Himeno M, Hamilton SR, August JT: Expression of lysosome-associated membrane proteins in human colorectal neoplasms and inflammatory diseases. Am J Pathol 2001, 159:449—455
24. Fortunato F, Bürgers H, Bergmann F, Rieger P, Büchler MW, Kroemer G, Werner J: Impaired autolysosome formation correlates with Lamp-2 depletion: role of apoptosis, autophagy, and necrosis in pancreatitis. Gastroenterology 2009, 137:350—360, 360.e1-5
25. Peschel A, Basu N, Benharkou A, Brandes R, Brown M, Dieckmann R, Rees AJ, Kain R: Autoantibodies to hLAMP-2 in ANCA-negative pauci-immune focal necrotizing GN. J Am Soc Nephrol 2014, 25: 455—463
26. Komatsu M, Waguri S, Chiba T, Murata S, Iwata J, Tanida I, Ueno T, Koike M, Uchiyama Y, Kominami E, Tanaka K: Loss of autophagy in the central nervous system causes neurodegeneration in mice. Nature 2006, 441:880—884
27. Hara T, Nakamura K, Matsui M, Yamamoto A, Nakahara Y, Suzuki-Migishima R, Yokoyama M, Mishima K, Saito I, Okano H, Mizushima N: Suppression of basal autophagy in neural cells causes neurodegenerative disease in mice. Nature 2006, 441:885—889
28. Di Malta C, Fryer JD, Settembre C, Ballabio A: Astrocyte dysfunction triggers neurodegeneration in a lysosomal storage disorder. Proc Natl Acad Sci U S A 2012, 109:E2334—E2342
29. Dehay B, Martinez-Vicente M, Caldwell GA, Caldwell KA, Yue Z, Cookson MR, Klein C, Vila M, Bezard E: Lysosomal impairment in Parkinson's disease. Mov Disord 2013, 28:725—732
30. Subramaniam SR, Chesselet MF: Mitochondrial dysfunction and oxidative stress in Parkinson's disease. Prog Neurobiol 2013, 106-107: 17—32
31. Cuervo AM, Stefanis L, Fredenburg R, Lansbury PT, Sulzer D: Impaired degradation of mutant alpha-synuclein by chaperone-mediated autophagy. Science 2004, 305:1292—1295
32. Kiffin R, Christian C, Knecht E, Cuervo AM: Activation of chaperone-mediated autophagy during oxidative stress. Mol Biol Cell 2004, 15: 4829—4840
33. Vogiatzi T, Xilouri M, Vekrellis K, Stefanis L: Wild type alpha-synuclein is degraded by chaperone-mediated autophagy and macroautophagy in neuronal cells. J Biol Chem 2008, 283: 23542—23556
34. Xilouri M, Brekk OR, Stefanis L: Alpha-synuclein and protein degradation systems: a reciprocal relationship. Mol Neurobiol 2013, 47:537—551
35. Tsuchiya Y, Okuno Y, Hishinuma K, Ezaki A, Okada G, Yamaguchi M, Chikuma T, Hojo H: 4-Hydroxy-2-nonenal-modified glyceraldehyde-3-phosphate dehydrogenase is degraded by cathepsin G. Free Radic Biol Med 2007, 43:1604—1615

BRIEF COMMUNICATION

De novo *KCNT1* mutations in early-onset epileptic encephalopathy

*†Chihiro Ohba, ‡[1]Mitsuhiro Kato, ‡Nobuya Takahashi, §¶Hitoshi Osaka, #Takashi Shiihara, **Jun Tohyama, ††Shin Nabatame, ††Junji Azuma, ‡‡Yuji Fujii, §§¶¶Munetsugu Hara, ##Reimi Tsurusawa, ##Takahito Inoue, ***Reina Ogata, ¶¶Yoriko Watanabe, †††Noriko Togashi, *Hirofumi Kodera, *Mitsuko Nakashima, *Yoshinori Tsurusaki, *Noriko Miyake, †Fumiaki Tanaka, *Hirotomo Saitsu, and *Naomichi Matsumoto

Epilepsia, 56(9):e121–e128, 2015
doi: 10.1111/epi.13072

Chihiro Ohba, a neurologist, is interested in genetic factors causing neurodevelopmental disorders.

Summary

***KCNT1* mutations have been found in epilepsy of infancy with migrating focal seizures (EIMFS; also known as migrating partial seizures in infancy), autosomal dominant nocturnal frontal lobe epilepsy, and other types of early onset epileptic encephalopathies (EOEEs). We performed *KCNT1*-targeted next-generation sequencing (207 samples) and/or whole-exome sequencing (229 samples) in a total of 362 patients with Ohtahara syndrome, West syndrome, EIMFS, or unclassified EOEEs. We identified nine heterozygous *KCNT1* mutations in 11 patients: nine of 18 EIMFS cases (50%) in whom migrating foci were observed, one of 180 West syndrome cases (0.56%), and one of 66 unclassified EOEE cases (1.52%). *KCNT1* mutations occurred de novo in 10 patients, and one was transmitted from the patient's mother who carried a somatic mosaic mutation. The mutations accumulated in transmembrane segment 5 (2/9, 22.2%) and regulators of K^+ conductance domains (7/9, 77.8%). Five of nine mutations were recurrent. Onset ages ranged from the neonatal period (<1 month) in five patients (5/11, 45.5%) to 1–4 months in six patients (6/11, 54.5%). A generalized attenuation of background activity on electroencephalography was seen in six patients (6/11, 54.5%). Our study demonstrates that the phenotypic spectrum of de novo *KCNT1* mutations is largely restricted to EIMFS.**

KEY WORDS: *KCNT1*, De novo mutation, Epilepsy of infancy with migrating focal seizures, Early onset epileptic encephalopathies.

Early onset epileptic encephalopathies (EOEEs) present with developmental impairment and intractable seizures from early infancy.[1] EOEEs include Ohtahara syndrome (OS), West syndrome, Dravet syndrome, epilepsy of infancy with migrating focal seizures (EIMFS; also known as migrating partial seizures in infancy), and other diseases.[2]

Accepted June 8, 2015; Early View publication July 3, 2015.

*Department of Human Genetics, Graduate School of Medicine, Yokohama City University, Yokohama, Japan; †Department of Clinical Neurology and Stroke Medicine, Yokohama City University, Yokohama, Japan; ‡Department of Pediatrics, Yamagata University Faculty of Medicine, Yamagata, Japan; §Division of Neurology, Clinical Research Institute, Kanagawa Children's Medical Center, Yokohama, Japan; ¶Department of Pediatrics, Jichi Medical School, Shimotsuke, Tochigi, Japan; #Department of Neurology, Gunma Children's Medical Center, Shibukawa, Japan; **Department of Pediatrics, Epilepsy Center, Nishi-Niigata Chuo National Hospital, Niigata, Japan; ††Department of Pediatrics, Osaka University Graduate School of Medicine, Osaka, Japan; ‡‡Department of Pediatrics, Hiroshima University Hospital, Hiroshima, Japan; §§Department of Neonatology, Medical Center for Maternal and Child Health, St. Mary's Hospital, Kurume, Japan; ¶¶Department of Pediatrics and Child Health, Kurume University School of Medicine, Kurume, Japan; ##Department of Pediatrics, Fukuoka University Chikushi Hospital, Fukuoka, Japan; ***Department of Pediatric Neurology, Fukuoka Children's Hospital, Fukuoka, Japan; and †††Department of Neurology, Miyagi Children's Hospital, Sendai, Japan

[1] Present address: Department of Pediatrics, Showa University School of Medicine, Tokyo, Japan.

Address correspondence to Hirotomo Saitsu and Naomichi Matsumoto, Department of Human Genetics, Graduate School of Medicine, Yokohama City University, 3-9 Fukuura, Kanazawa-ku, Yokohama 236-0004, Japan. E-mails: hsaitsu@yokohama-cu.ac.jp and naomat@yokohama-cu.ac.jp

Table 1. Clinical features of patients with *KCNT1* mutations

Clinical feature	Patient number										
	1	2	3	4	5	6	7	8	9	10	11
Age	6 y 0 mo	3 y 7 mo	5 y 4 mo	1 y 10 mo	2 y 3 mo	6 y 2 mo	5 y 3 mo	2 y 6 mo	1 y 2 mo	1 y 4 mo	4 y 3 mo
Sex	Male	Female	Female	Male	Male	Male	Male	Female	Female	Male	Male
Diagnosis	EIMFS (or OS)	EIMFS	EIMFS	EIMFS	EIMFS	EIMFS	EIMFS	West	EIMFS	EIMFS	EOEE
Mutation	c.1420C>T de novo	c.808C>G de novo	c.1225C>T de novo	c.862G>A de novo	c.1421G>A de novo	c.2800G>A de novo	c.1421G>A de novo	c.1421G>A de novo	c.2771C>T inherited[a]	c.1429G>A de novo	c.1283G>A de novo
Initial symptom	Tremor	Seizure	Seizure	Seizure	Poor feeding	Seizure	Seizure	Seizure	Seizure	Seizure	Seizure
Age at onset	0 days	2 days	2 mo	4 mo	1 mo	4 days	15 days	2 mo	1.5 mo	1–2 weeks	1 mo
Epileptic seizures	Facial flushing with TS from 20 days. Clusters of blinking with eye deviation and TS from 1 mo	Clonic seizure, oral automatism, eye deviation	Focal seizure	Eye deviation only or followed by TS	Bilateral eyelid twitching and stiffness of bilateral upper limbs	Clonic seizure starting from various lesions	TS and head and eye deviation, automatic seizure	Epileptic spasms at 2 mo, TS at 6 mo	TS and postural seizure	Eye deviation followed by postictal automatisms	Staring and right hemiclonic seizure
Initial EEG	Normal at 2 days	Multifocal polyspikes or sp-w with focus migration, brief period of suppression	Focal spikes	Diffuse high-amplitude slow wave, multifocal sp-w or sharp and slow wave	Multifocal polyspikes, sp-w, Hyps with de-synchronization	Multifocal polyspikes, sp-w	Focal spikes with de-synchronization	Irregular polyspikes, sp-w, Hyps with de-synchronization	Diffuse high-voltage slow wave, multifocal sp-w	Normal	Focal sharp wave at C3
Follow-up EEG	MFS, sp-w and polyspike at 1 mo. Multifocal polyspikes with periodic slow wave similar to Hyps during awake and SB pattern during sleep		Multifocal polyspikes (O dominant)	Continuous polymorphous-amplitude slow wave with no paroxysmal discharges at 14 mo	Focal sharp waves, continuous slow waves/ sharp and slow waves, SB pattern during sleep	Diffuse slow waves	Diffuse slow waves	Low voltage background with single spike at frontal to central area	Prominent slow waves without synchronicity and MFS or spike and slow wave complexes similar to Hyps	Abnormal background, MFS, spike and waves	MFS, Brief period of suppression
Ictal EEG	Polyspikes followed by diffuse rhythmic waves		Focal rhythmic waves. Burst of spike and waves	Migrating rhythmic sharp θ or α activity followed by irregular sp-w	Migrating rhythmic sharp θ or α activity, burst of spike and waves	Migrating rhythmic sharp θ or α activity, burst of spike and waves	Migrating focal polyspikes			Frequent spikes originating from left or right side separately	Rhythmic δ wave activity at bilateral occipital area
Migrating foci	F3–F4 to P3–P4	F3, F7, Fp1 to T5, O1, T3	C4, T4 to T5, O1	O2 to T5, P3	Left or right hemisphere to contralateral side	T5, T3 to C3, F3 to O1	Left or right F-C to contralateral side	None	F4, C4, F8, T6 to P3, C3, F3, T3	T3 to T4 or T4 to T3, P3	None

Continued